Assessment of the quality of the Version 1.07 temperature-versus-pressure profiles of the middle atmosphere from TIMED/SABER

E. E. Remsberg,[1] B. T. Marshall,[2] M. Garcia-Comas,[3] D. Krueger,[4] G. S. Lingenfelser,[5] J. Martin-Torres,[5] M. G. Mlynczak,[1] J. M. Russell III,[6] A. K. Smith,[7] Y. Zhao,[8] C. Brown,[2] L. L. Gordley,[2] M. J. Lopez-Gonzalez,[3] M. Lopez-Puertas,[3] C.-Y. She,[4] M. J. Taylor,[8] and R. E. Thompson[2]

Received 22 February 2008; revised 5 June 2008; accepted 24 June 2008; published 3 September 2008.

[1] The quality of the retrieved temperature-versus-pressure (or $T(p)$) profiles is described for the middle atmosphere for the publicly available Sounding of the Atmosphere using Broadband Emission Radiometry (SABER) Version 1.07 (V1.07) data set. The primary sources of systematic error for the SABER results below about 70 km are (1) errors in the measured radiances, (2) biases in the forward model, and (3) uncertainties in the corrections for ozone and in the determination of the reference pressure for the retrieved profiles. Comparisons with other correlative data sets indicate that SABER $T(p)$ is too high by 1–3 K in the lower stratosphere but then too low by 1 K near the stratopause and by 2 K in the middle mesosphere. There is little difference between the local thermodynamic equilibrium (LTE) algorithm results below about 70 km from V1.07 and V1.06, but there are substantial improvements/differences for the non-LTE results of V1.07 for the upper mesosphere and lower thermosphere (UMLT) region. In particular, the V1.07 algorithm uses monthly, diurnally averaged CO_2 profiles versus latitude from the Whole Atmosphere Community Climate Model. This change has improved the consistency of the character of the tides in its kinetic temperature (T_k). The T_k profiles agree with UMLT values obtained from ground-based measurements of column-averaged OH and O_2 emissions and of the Na lidar returns, at least within their mutual uncertainties. SABER T_k values obtained near the mesopause with its daytime algorithm also agree well with the falling sphere climatology at high northern latitudes in summer. It is concluded that the SABER data set can be the basis for improved, diurnal-to-interannual-scale temperatures for the middle atmosphere and especially for its UMLT region.

Citation: Remsberg, E. E., et al. (2008), Assessment of the quality of the Version 1.07 temperature-versus-pressure profiles of the middle atmosphere from TIMED/SABER, *J. Geophys. Res.*, *113*, D17101, doi:10.1029/2008JD010013.

1. Introduction

[2] The Sounding of the Atmosphere using Broadband Emission Radiometry (SABER) experiment was launched on the Thermosphere-Ionosphere-Mesosphere Energetics and Dynamics (TIMED) satellite in December 2001 [*Russell et al.*, 1999]. The primary goal of SABER has been to obtain profile measurements of parameters and species related to the thermal structure and energetics of the upper mesosphere and lower thermosphere (UMLT) region of the atmosphere. To achieve that objective, its infrared limb radiance profiles need to be free of instrument effects and registered accurately throughout the middle atmosphere (~10 to 100 km), prior to the retrieval of its primary geophysical quantities. Because the SABER measurement and retrieval concept has its heritage from the Nimbus 7 Limb Infrared Monitor of the Stratosphere (LIMS) experiment [see *Gille and Russell*, 1984, and references therein], the reader is also referred to the descriptions of the forward model and the potential error mechanisms for the retrieved temperature profiles from the most recent Version 6 (V6) of that data set [*Remsberg et al.*, 2004].

[3] SABER views 90° to the right of the velocity vector of the TIMED spacecraft. The daily longitude-versus-latitude coverage for the SABER tangent point locations vary

[1]Science Directorate, NASA Langley Research Center, Hampton, Virginia, USA.
[2]G & A Technical Software, Inc., Newport News, Virginia, USA.
[3]Instituto de Astrofisica de Andalucia, CSIC, Granada, Spain.
[4]Department of Physics, Colorado State University, Fort Collins, Colorado, USA.
[5]Science Systems and Applications, Inc., Hampton, Virginia, USA.
[6]Center for Atmospheric Sciences, Hampton University, Hampton, Virginia, USA.
[7]National Center for Atmospheric Research, Boulder, Colorado, USA.
[8]Center for Atmospheric and Space Sciences, Utah State University, Logan, Utah, USA.

0148-0227/08/2008JD010013

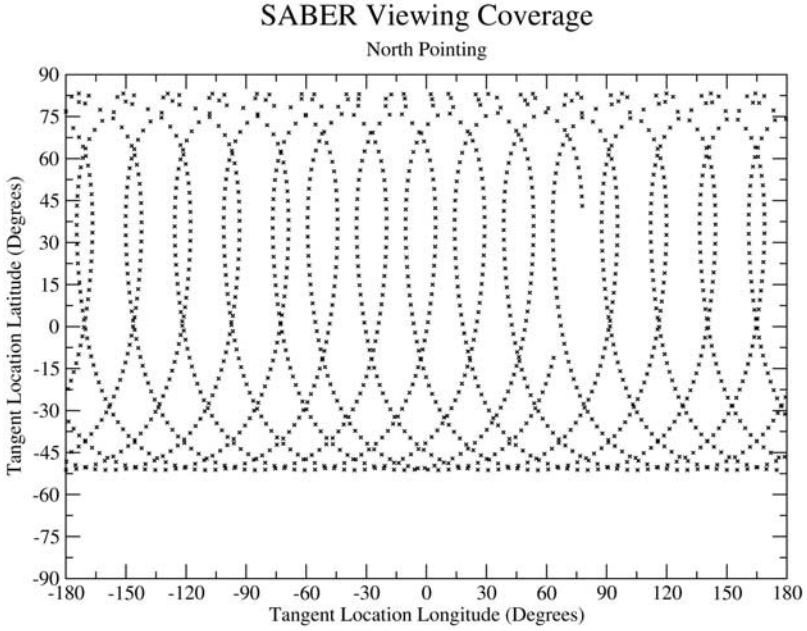

Figure 1. Latitude-versus-longitude tangent point locations for one day of observations from Sounding of the Atmosphere using Broadband Emission Radiometry (SABER) in its north viewing phase (83°N to 52°S).

along the orbit from 83°N to 52°S for the north viewing, yaw mode of the spacecraft, as shown in Figure 1. Its north viewing mode extends for 60 to 63 days. The spacecraft is turned to its south viewing mode for another 60+ days, and then the entire viewing sequence is repeated. The tangent track pattern of Figure 1 flips top to bottom for the SABER south viewing mode. Thus, there is essentially continuous coverage for the latitudes of 52°N to 52°S, while the higher latitudes are viewed for alternating 60+ day periods. Yaw events occur on nearly the same dates for each succeeding year.

[4] Vertical profiles of retrieved temperature as a function of pressure, hereinafter $T(p)$, and their derived geopotential height and wind distributions were presented for an initial, local thermodynamic equilibrium or LTE Version 1.01 (V1.01) of the SABER data of *Remsberg et al.* [2003]. Climatological profiles of the minor interfering and unobserved species were obtained from the model of *Garcia and Solomon* [1994]. Although those early results were shown to be of good quality, some important improvements were made for the calibration and conditioning of the observed radiances in V1.02 through V1.04 [*Mertens et al.*, 2002, 2004]. Non-LTE (NLTE) algorithms for kinetic temperature (T_k) were employed in V1.03 [*Lopez-Puertas et al.*, 2004] and in the next two public data versions, V1.04 and V1.06 [*Mertens et al.*, 2004, 2008]. Both of those public versions made use of an iterative algorithm for the retrievals of both T_k and CO_2 during daytime, but obtained CO_2 from the Thermosphere-Ionosphere-Mesosphere Electrodynamics General Circulation Model (TIME-GCM) [*Roble and Ridley*, 1994] for nighttime. V1.04 employed profiles of $O(^3P)$, $O(^1D)$, and other neutral molecules from TIME-GCM for its retrieval of T_k. V1.06 used SABER-derived values of $O(^3P)$ and $O(^1D)$; however, in the thermosphere those values were obtained from the Mass Spectrometer Incoherent Scatter model, MSIS-90 of *Hedin* [1991]. A number of improvements were made in the calculation of the forward radiances and for the registration of the observed radiances with pressure altitude for V1.06. They included the addition of line mixing for the 15-μm CO_2 band models and the use of an average interleave procedure for profile registration (see later). In addition, much less smoothing was employed in the calculation of the vibrational temperatures below 100 km and for the retrieval of T_k.

[5] This paper begins by describing the quality of the SABER V1.07 CO_2 channel radiances and its retrieved $T(p)$ for the stratosphere and lower mesosphere (below 65 km), where the forward radiance model is based on LTE assumptions. Next, the V1.07 results from the more complex, NLTE model are evaluated in terms of the retrieval of T_k above 65 km and through the UMLT region; previous assessments of the SABER NLTE algorithms and of T_k can be found in the work of *Mertens et al.* [2001, 2002, 2004] and in the work of *Kutepov et al.* [2006]. There were inconsistencies in the vertical structure of the diurnal temperature tides from V1.04 and V1.06 because their daytime CO_2 values were retrieved, while their nighttime profiles were from a model. There were also computational instabilities introduced by the NLTE forward model for the 4.3-μm CO_2 radiance, leading to large differences in the solutions from one retrieval interleave to the next. Attempts to screen such occurrences resulted in far too many profiles being rejected. It is noted that very little of the radiance for this channel comes from tangent layers near the mesopause. Instead, the V1.07 T_k has been obtained for both day and night using monthly and diurnally averaged CO_2 profiles from the distributions with latitude in the Whole Atmosphere Community Climate Model (WACCM) [*Garcia et al.*, 2007] (see also section 3). A detailed description of the V1.07 NLTE algorithm and estimates of the error for T_k are given in a forthcoming paper (M. Garcia-Comas et al.,

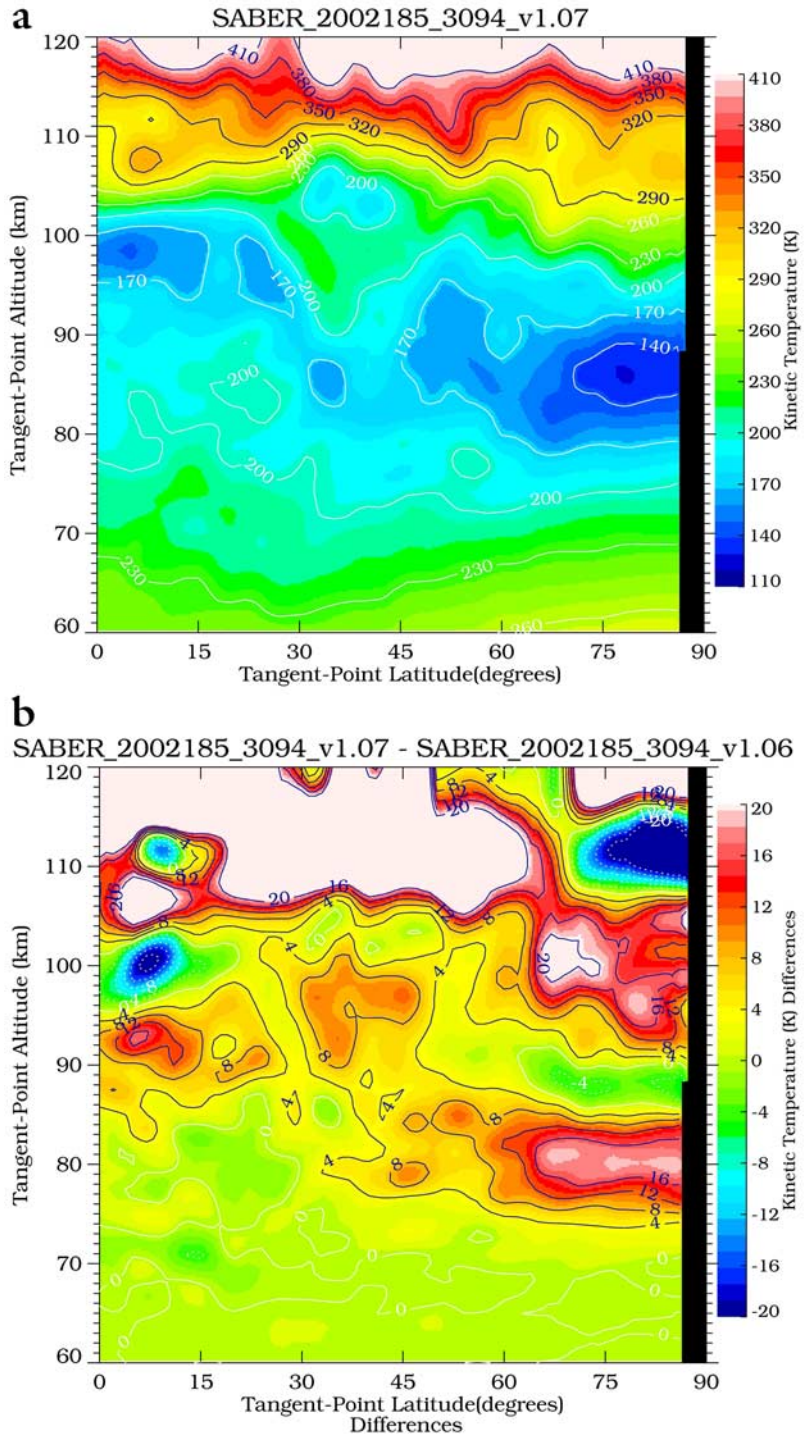

Figure 2. (a) SABER V1.07 temperature distribution for a daytime orbital segment of the Northern Hemisphere on 4 July 2002. Contour interval is 30 K. (b) Temperature differences (in K) for 4 July 2002: V1.07 minus V1.06. Contour interval is 4 K.

Errors in SABER kinetic temperature caused by non-LTE model parameters, submitted to *Journal of Geophysical Research*, 2008).

[6] Some representative V1.07 results are shown in Figures 2a and 2b at this juncture for a test day, 4 July 2002, of a north viewing period for SABER that also occurred during the summer component of a MaCWAVE/MIDAS ground-based field campaign for characterizing atmospheric dynamics in the region of the Arctic polar mesopause [*Goldberg et al.*, 2004]. Figure 2a is a plot of the temperature distribution of the mesosphere and lower thermosphere for a daytime orbital segment. The basic temperature structure of the UMLT is captured well by SABER, including the cold mesopause that changes in altitude near

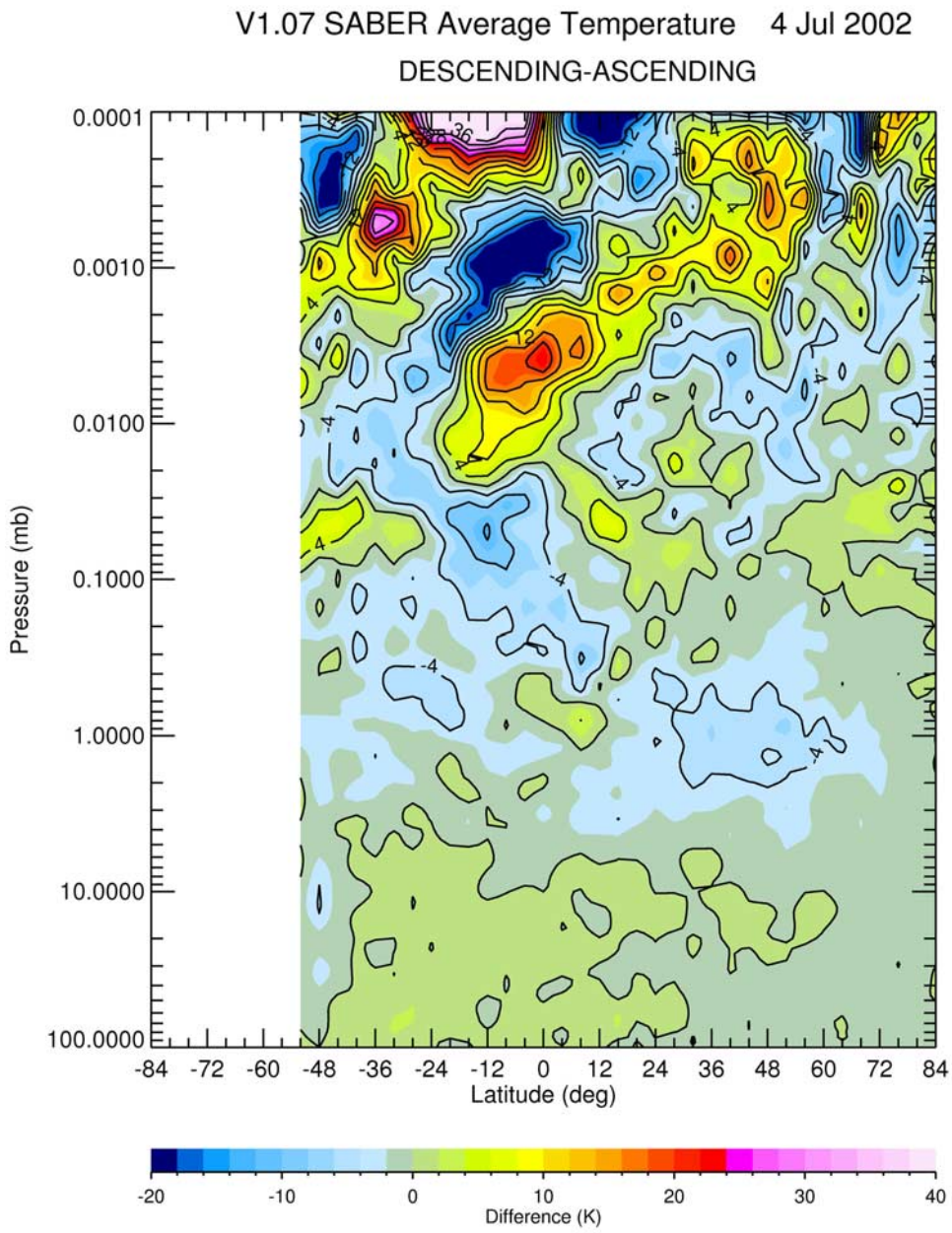

Figure 3. Zonal-mean cross section of the descending minus ascending SABER temperatures for 4 July 2002. Contour interval is 4 K.

35°N. On the basis of the work of *Kutepov et al.* [2006], the NLTE forward model was updated to account for the redistribution of the ν_2 quanta among the first excited levels of the various CO_2 isotopes. That addition for V1.07 has had a significant impact in the region of the cold summer mesopause and to a lesser extent in the region of the tropical mesopause (Garcia-Comas et al., submitted manuscript, 2008). To illustrate those changes, Figure 2b is the V1.07 (Figure 2a) minus V1.06 $T(p)$ distribution. A net effect is that the polar mesopause from V1.07 is warmer and several kilometers higher than that from V1.06 (see also section 5).

[7] Figure 3 shows the zonal average differences from the descending minus ascending orbital distributions for SABER $T(p)$ on 4 July 2002; the differences for this date correspond to nighttime minus day etween about 20°S and 60°N latitude and occur nearly half a day apart. One can see clearly the vertical variations in $T(p)$ at the lower latitudes due to the diurnal tide; the tidal phase is changing with latitude for selected constant pressure altitudes as expected, particularly for the mesosphere. There is even a weak positive difference for the lower latitudes of the lower stratosphere (night > day), and its pattern is nearly hemispherically symmetric across the tropical latitudes. We have verified through statistical tests that the position and three-axis velocity information from the ephemeris of TIMED indicate that the motions of the spacecraft are too small to impart any significant variations onto the radiances and retrieved $T(p)$. Thus, it is presumed that the patterns of descending minus ascending differences are real in Figure 3. The vertical variations of the differences due to the tides also

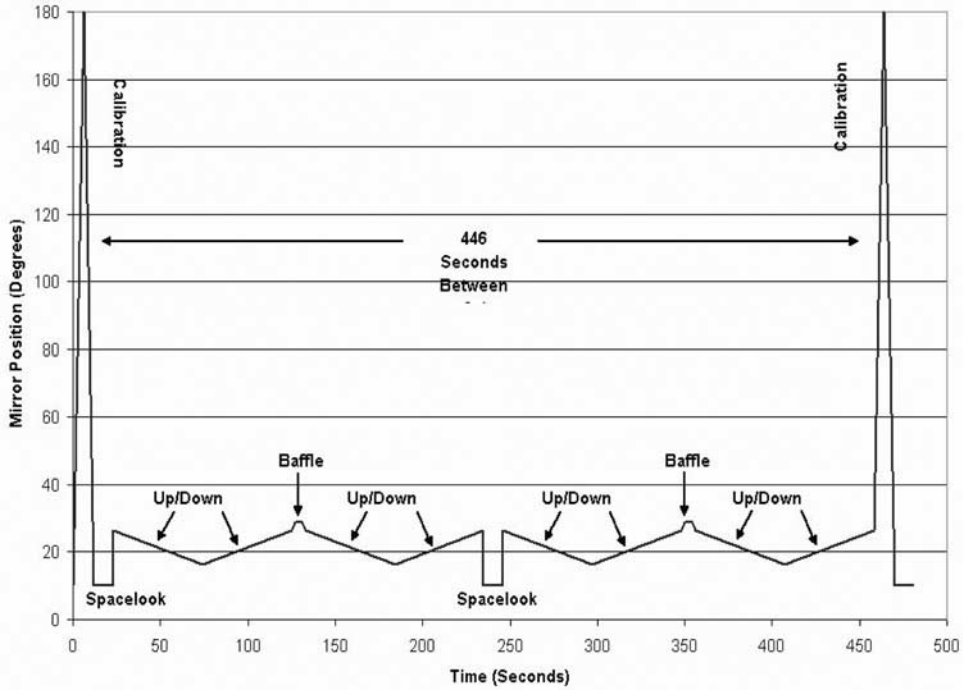

Figure 4. SABER in-flight calibration and scan-mirror sequence. Space-look counts are obtained every 3.5 min (see text for more details).

change slowly for successive days (not shown), as the local times of the ascending and descending tangent tracks undergo their precession over the period of the yaw cycle. However, one should not conclude from the results of Figure 3 that effects of horizontal temperature gradients are unimportant for the high northern latitudes because in that instance SABER was viewing in nearly the same direction for both its ascending and its descending orbital segments.

[8] For instance, for Figures 2a and 3 the SABER instrument was looking in the direction of the positive, horizontal gradient for $T(p)$ at the stratopause when making measurements poleward of about 60°N, but along its negative gradient at the mesopause. The SABER operational algorithm does not account for the second-order effects of those gradients, as was done with the two-pass retrieval approach used for the LIMS V6 temperatures. At low and middle latitudes SABER views in a more nearly east/west direction, where the signs of the horizontal gradients of $T(p)$ and their effects for the retrieval of $T(p)$ are more variable and depend on the phase of the zonal planetary temperature wave at the tangent point longitude. Thus, the effects of horizontal gradients tend to cancel out for zonal averages of $T(p)$ at those latitudes. Zonal wave amplitudes are small for the stratosphere and mesosphere when there are summer easterlies [*Andrews et al.*, 1987]; gradient corrections are not needed for even the individual SABER $T(p)$ profiles of the middle latitudes at those times.

[9] SABER has improved upon LIMS in other respects, as will be noted in sections 2 and 3. Rather than conducting a comprehensive assessment of all possible errors for the SABER $T(p)$ in this paper, an assessment is provided of the known, primary sources of its systematic errors. In addition, appropriate diagnostics are obtained from the data themselves and from some c risons with several other well-characterized data sets, in order to illustrate whether those errors are underestimates. Section 2 describes the observed radiances from the SABER 15-μm CO_2 channels. Section 3 is a review of the uncertainties for the forward model, the measured radiances and their temperature retrievals for both the LTE and NLTE algorithms. In addition, it describes the variability of the retrieved $T(p)$ and compares it with similar estimates of the random error due to the measurement noise for the SABER CO_2 channels. Section 4 contains an assessment of the primary sources of its systematic errors, based on some comparisons versus distributions of the lower vertical resolution $T(p)$ from the Advanced Microwave Sounding Unit (AMSU) instruments onboard the operational NOAA satellites. Section 4 also shows sets of profile comparisons with soundings from the Michelson Interferometer for Passive Atmospheric Sounding (MIPAS) experiment on Envisat, from ground-based Rayleigh lidar, and from the Halogen Occultation Experiment (HALOE) of the Upper Atmosphere Research Satellite (UARS). Section 5 reports on the quality of the results from the V1.07 NLTE algorithm by showing T_k comparisons with the falling sphere climatology of *Lübken* [1999] and with several sets of ground-based, correlative measurements for the UMLT region. Section 5 also indicates that the V1.07 NLTE algorithm has led to $T(p)$ values that are more consistent than those from V1.06 for diagnosing tidal signatures in the UMLT region. Section 6 summarizes the findings about the quality of the SABER distributions of $T(p)$.

2. Measurement and Conditioning of Radiances From the 15-μm CO_2 Channels

[10] Figure 4 is a schematic of the scan sequence that was employed for the SABER measurements. The sequence

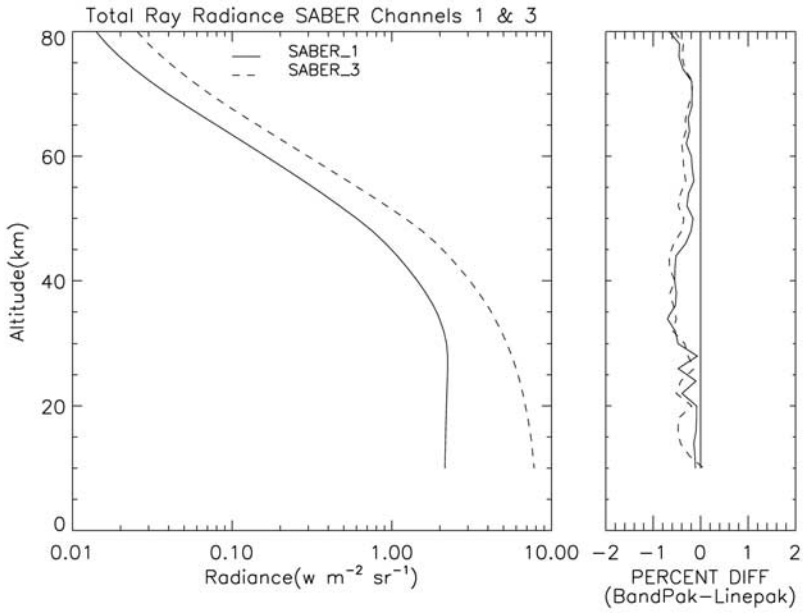

Figure 5. (left) Low-altitude portions of forward radiance profiles for SABER channels (Chs) 1 and 3. (right) Radiance difference profiles (in percent): band model minus line-by-line results.

begins with an acquisition scan (from "space-look" to horizon) extending over a range of 16.3° followed by an up/down, adaptive scan that spans 5.8°. A four-scan data collection sequence is made, beginning with a look at the internal flight calibration (IFC) blackbody that is kept at a temperature of about 247 K and followed by a view to cold space. Then, an up/down adaptive scan-pair measurement is performed, followed by a view of the radiance from the direction of the instrument baffling that is used to obtain estimates of internal stray light effects. A second up/down pair and a "space-look" are obtained next, and then the whole sequence is repeated. There is also an option for obtaining additional radiance measurements during a large-angle sweep of the scan mirror.

[11] The SABER measurement and retrieval for $T(p)$ follow closely with the iterative, narrow (CO_2N) and wide (CO_2W) 15-μm channel approach of LIMS [*Gille and House*, 1971; *Gille et al.*, 1984; *Remsberg et al.*, 2004]. The CO_2 filter positions and widths for SABER are very similar to those of LIMS. The narrow channel (or Ch 1) of SABER extends from 649–698 cm^{-1}, and its wide channel (or Ch 3) extends from 580–763 cm^{-1} (wave numbers where the transmissions of the filters drop to 5%) [*Russell et al.*, 1999]. It is noted that the SABER instrument actually has 2 wide CO_2 15-μm channels (Chs 2 and 3) of similar spectral extent for the original purpose of diagnosing and correcting for the effects of spacecraft motion within each successive up/down pair of radiance scans along the orbits. However, only the forward radiances for Ch 3 were iterated along with those of Ch 1 for the actual retrieval of $T(p)$ because the spectral responses for Chs 2 and 3 were not as similar as planned.

[12] The orbital attitude of the TIMED spacecraft (and of SABER) is obtained using star trackers and/or inertial navigation gyros (ING). The wide-channel CO_2 profiles from Chs 2 and 3 were checked for any evidence of slow, mean spacecraft motion would affect an up and a down scan differently. Specifically, the $T(p)$ obtained from the radiance profile of Ch 3 was used to calculate the forward radiance profile for Ch 2. The calculated radiance was subtracted from the measured radiance for Ch 2, and the profiles of their residuals were examined. In almost all cases the residuals were quasi-random and very small. However, the SABER scan mirror can also be affected by high-frequency, spacecraft vibrations or "jitter" that nominally lead to profile registration errors of ±20 m. Checks of the point-to-point changes for the scan angles were made in the Level 1 software to eliminate any profiles that had point-to-point mirror motions of 5 times nominal scan rate or that showed a reversal. Less than 2% of all the profiles were screened out and not processed further because of these criteria. In general, there is consistency for the small-scale, vertical radiance (and temperature) variations among the SABER channels, indicating the presence of tides, gravity waves, and inversion layers within the atmosphere. The effects of jitter are included in the estimates of total random error for LTE results, but are a negligible fraction of the total NLTE error in the UMLT (section 3).

[13] The SABER measurements offer a number of advantages over their heritage from the LIMS experiment. For example, the SABER in-orbit detector noise values for the narrow and wide channels are much smaller—by a factor of 5.4 for Ch 1 or 2.57×10^{-4} W/(sr-m^2) and by a factor of 16.8 for Ch 3 or 3.28×10^{-4} W/(sr-m^2). That reduction in the noise is despite the fact that the focal plane array (FPA) for the SABER detectors is being maintained at a temperature of about 74 K by its cryocooler; the LIMS FPA was maintained at 63 K. Thus, the reduced noise of SABER is due largely to enhancements in detector technology over the past several decades, providing for the extension of useful 15-μm CO_2 limb radiance profile information well into the lower thermosphere.

[14] The middle atmosphere portion of the radiance profiles is shown for Chs 1 and 3 in Figure 5. Ch 3 has

signal-to-noise (S/N) of about 100 at 80 km and 3000 at 50 km, the latter just above the top of the altitude range (15 to 2 hPa) where its profile registration with pressure is performed. The radiance profile varies linearly in log pressure in the mesosphere and upper stratosphere, which is also where it is most sensitive to uncertainties for the removal of instrument effects and for its registration. Because Ch 3 continues to see the increasing radiances from the weaker CO_2 lines of the lower altitudes, its temperature information can be retrieved with excellent vertical resolution in the lower stratosphere, too. The accuracy of its retrieved profile depends on the biases for its forward radiance model both at and above the tangent layer, as indicated in the right profile of Figure 5 and discussed in more detail in section 3.

[15] The Ch 1 radiance profile of Figure 5 has vertical gradients that are very similar to those of Ch 3 above about 40 km, but its S/N is only about 50 at 80 km and 2000 at 50 km. Its radiance profile becomes very nonlinear in the region of its ''knee'' near 30 km, or below where its signal is nearly constant with altitude [*Gille and House*, 1971]. Its radiances in the lower stratosphere are mostly from the near-saturated, center portions of the 15-μm CO_2 bands. There is little information about $T(p)$ below the ''knee'' from the radiances of Ch 1, other than that provided by its vertical instantaneous field of view (IFOV) of the limb. The IFOV widths for SABER Ch 1 and Ch 3 are 1.68 km and 1.49 km, respectively. In addition, there is a close correspondence between the IFOV widths for the channels used to obtain $T(p)$, ozone and water vapor on SABER, which allows for calculations of the effects of the temperature structure in the forward radiances of ozone and water vapor with hardly any prior smoothing of the $T(p)$. For this reason the SABER measurement and algorithm accounts for much of the temperature variations in those species radiances, arising from atmospheric tides and/or gravity waves. The successive up and down scans along an orbit are not averaged prior to their retrieval, contrary to the approach used for LIMS to remove the effects of intermediate-scale motions of the Nimbus 7 spacecraft. Thus, it is also easier to ''sense'' the vertical structure in the individual SABER temperature profiles due to the effects of the atmospheric tides and gravity waves because those temporal changes are not being averaged and dampened [e.g., *Preusse et al.*, 2006].

[16] The CO_2 channels obtain radiance measurements over a very large dynamic range, especially through the mesosphere. Preflight, laboratory calibration measurements were performed for the SABER channels over a wide spectral range to check for any out-of-band spectral features; no perceptible filter ''leakage'' was found. The off-axis, spatial FOV and the low-pass, electronics filter responses were also carefully measured in the lab for each channel and then deconvolved from the observed radiances within the SABER Level 1 software. Checks were made for the presence of spatial FOV sidelobes due to any off-axis scatter internal to the SABER instrument by analyses of in-orbit, limb scans across the Moon, which represents a well-known, finite source function. The results from those Moon scans are of very good quality, and they were combined with the laboratory test measurements for defining the final FOV functions for each channel. In general, it was found that the effects of the instrument were characterized very well for the CO nels, prior to the launch of SABER, and that they are deconvolved accurately from the radiances in the Level 1 software.

[17] The observed radiances were corrected for offsets on the basis of laboratory measurements of the IFC blackbody. Soon after SABER began making observations it became clear that there were slight (few percent), unexplained biases in those measured radiances, and it was realized that the effects of the temperature of the FPA had not been accounted for properly during the laboratory measurements of the instrument ''blackbody'' (or IFC). Significant improvements were obtained for the retrieved $T(p)$, 9.6-μm ozone, and water vapor of V1.01, as a result of applying those corrections to the SABER radiances. The effects of radiance bias errors for $T(p)$ are discussed in section 3.

[18] The measured CO_2 radiances were calibrated further on the basis of the along-orbit responses of the channels to the IFC and space views of the scan sequences (see Figure 4). However, four months into the mission it was found that the responses of Chs 1, 2, and 3 had decreased to about 74% of their initial values. It was concluded that this behavior was due to a deposit of a thin layer of ice on the cooled FPA, as a result of the initial outgassing of residual moisture from the instrument and from the spacecraft once in orbit. That situation was alleviated by turning off the power to the SABER cryocooler temporarily, which allowed the FPA and the detectors to warm up and the ice film to sublime quickly. Then, the cryocooler was powered back on, returning the detectors to their low operating temperatures and normal response levels. After May 2002 the detector responses were monitored and the cryocooler cycled off and then back on again whenever the Ch 1 response decreased to 95% of its initial value. This procedure worked very well; it was applied initially in May and then about every 2 months in 2002. By 2007 it was needed only once per year, presumably because the water molecules became outgassed and dispersed over time. Simulations of the spectral effects of an ice film indicate that the 15-μm region would be affected the most, but no clear evidence of any anomalies in the retrieved temperatures was found even for those early months. In all other respects the SABER instrument has maintained its nominal operating characteristics to the present time. Thus, it is believed that SABER is providing high-quality measurements for the purpose of resolving the interannual terms and eventually the solar-cycle response of its temperature time series.

3. Forward Radiance Models and Retrieval Algorithms

3.1. LTE Algorithm and Uncertainties for $T(p)$

[19] Simulations were conducted to verify that the assumption of LTE is sufficiently adequate for the representation of the 15-μm radiance profiles in the lower mesosphere and certainly in the stratosphere, where the registration of the observed radiances with pressure is performed. The LTE forward model assumes that the CO_2 mixing ratio is constant throughout the middle atmosphere. Its value in the software was updated annually in accord with the observed rate of increase for CO_2 at the ground from NOAA monitoring sites, but lagged by 4 years to account for the slow ascent of that air to above the 10-hPa level. A band model approximation, BANDPAK, of

Table 1. Random and Systematic Errors for SABER Local Thermodynamic Equilibrium $T(p)$[a]

	Pressure (hPa)						
	100	50	10	3	1	0.4	0.1
Random (or Precision)							
Pointing jitter (±20 m)	0.3	0.3	0.3	0.6	0.6	0.6	0.5
Noise	0.1	0.1	0.1	0.1	0.2	0.3	0.5
Systematic (Accuracy)							
CO_2 forward model (<0.2–0.7%)	0.6	0.6	0.7	0.6	0.2	0.2	0.2
Ch 3 radiance error (+1%)	1.0	1.0	−0.1	−1.3	−1.6	−1.5	−1.0
Pressure registration shift (bottom, 15–10 hPa)	−0.5	−0.3	0.0	0.5	0.8	1.0	0.8
O_3 correction error (−10%)	−0.5	0.3	0.2	−0.1	−0.5	−0.7	−0.7
Root-sum-square (±) of random and bias errors	1.4	1.3	0.8	1.6	2.0	2.1	1.6

[a]Units are kelvins.

Marshall et al. [1994] was used for calculations of the forward radiances in the operational algorithm. BANDPAK is generally accurate to better than 1% when compared to the rigorous line-by-line (l-b-l) model, LINEPAK, of *Gordley et al.* [1994], as shown in Figure 5. CO_2 line parameters were taken from the HITRAN 2000 line list [*Rothman et al.*, 2003], and they are essentially unchanged in HITRAN 2004 for the broad band pass of the SABER channels. However, those line parameters were modified to account for the effects of CO_2 line coupling in its Q branch [*Rothman et al.*, 2005; *Niro et al.*, 2005; *Gordley et al.*, 1994], altering the forward radiances by as much as 1.2% for Ch 1 and 0.7% for Ch 3 at 40 km. The effects of line coupling for the adjacent P and R branches [*Niro et al.*, 2005] were not included in the forward model, but simulation studies show that their influence is not important above about 15 km. No other errors are assumed for the spectroscopic line parameters of CO_2.

[20] SABER Chs 1, 2, and 3 contain radiance contributions from ozone, N_2O, and water vapor, as well as CO_2, although water vapor is significant only for the troposphere. For Ch 1 the ozone accounts for about 25% of the total radiance at 20 km, decreasing to 15% at 30 km, 10% at 40 km, and about 5% at 50 km. The percentage contributions from ozone for Chs 2 and 3 are somewhat larger at 30 km (18%), at 40 km (14%), and at 50 km (10%), but slightly less at 20 km (23%). The distribution of N_2O is based on model climatology [*Garcia and Solomon*, 1994]; it represents the observed values very well in the lower stratosphere. N_2O contributes no more than 1% of the radiance in Chs 2 and 3 above 30 km, where its vertical gradients are large and its values can differ substantially from the climatology. There is also a very small ($\ll$1%) contribution from N_2O_5 that is not modeled. The 9.6-μm ozone channel (Ch 4) radiances also include contributions from the CO_2 laser bands in the middle mesosphere, but the deviations of those bands from LTE do not impact the determination of $T(p)$ f stratosphere.

[21] Emissivity tables based on the band model were calculated for CO_2, ozone, N_2O, and water vapor as functions of temperature, pressure, and mass path, and they were used for calculations of the rate of change of the emissivity along the limb-path LOS. As for the CO_2 channels of LIMS, there are significant interactions for the radiances from the stronger lines of CO_2 and the lines of the 14-μm ν_2 band of ozone in the stratosphere. Thus, additional emissivity tables were generated to account for their overlapping effects in the forward models of Chs 1 and 3 [*Marshall et al.*, 1994; *Remsberg et al.*, 2004]. A lower limit of 110 K was set for the retrieved temperatures of V1.07, owing to an arbitrary lower limit of 102 K for the temperature range of the emissivity tables.

[22] The SABER operational LTE retrieval algorithm has several steps, and they are based on the multiple interleave approach that was applied to the narrow and wide CO_2 channel radiances of LIMS V6 [*Remsberg et al.*, 2004]. Specifically, a profile is retrieved from a given radiance profile, based on every fifth point spaced by about 1.9 km or near the vertical resolution for the measurement. Four other independent retrievals are conducted, using the remaining points of the radiance profile but with each one shifted downward by one point. The five separate retrieved profiles are interpolated to the full grid of 0.375 km spacing and then averaged together—the interleave process. Initially, the observed radiance versus scan angle (or relative altitude) information of Chs 1 and 3 is converted to geopotential height (and then geometric altitude) on the basis of the current-day, 12Z analyses of the pressure at 30 km from NOAA/NCEP. Then, a determination of a reference pressure, p_o, and registration with pressure altitude is performed by iterating the calculated radiances against the measured radiances for Ch 1 for the stratospheric levels between 2 hPa and 15 hPa. First-pass, "onion-peel" retrievals for both $T(p)$ and ozone mixing ratio (or $O_3(p)$) are conducted using the Level 2 software and the observed Ch 3 and Ch 4 (9.6-μm ozone) radiance profiles, as registered with the initial pressure profile associated with the radiances of Ch 1. Those first-pass profiles for $T(p)$ and ozone are then used to recalculate forward radiances for Ch 1. A new pressure profile for the observed radiances of Chs 1, 3, and 4 is generated using an updated estimate for p_o. A second retrieval of the Ch 3 radiance-versus-pressure profile is performed to get an update for $T(p)$. These steps are iterated until they converge to final temperature and ozone profiles. The calculated and observed radiances are matched to within their estimated noise values.

[23] Table 1 contains estimates of the precision (random error) and accuracy for a single, retrieved U. S. Standard Atmosphere $T(p)$ profile. The primary source of random error in the stratosphere and lower mesosphere is pointing jitter; in the midmesosphere the effects of jitter and detector noise are comparable. Effects of jitter were adapted from *Remsberg et al.* [2004, Table 2]. There are also random uncertainties among the results of the 5 separate interleave solutions for each retrieved profile. Thus, the random errors for SABER in Table 1 are also the result of an average from the interleaves, which reduces the effects of the noise by $\sqrt{5}$ (or by a factor of 2.2).

[24] Figure 6 shows a profile of the standard deviation (SD) differences (dotted with diamonds) from sets of orbital

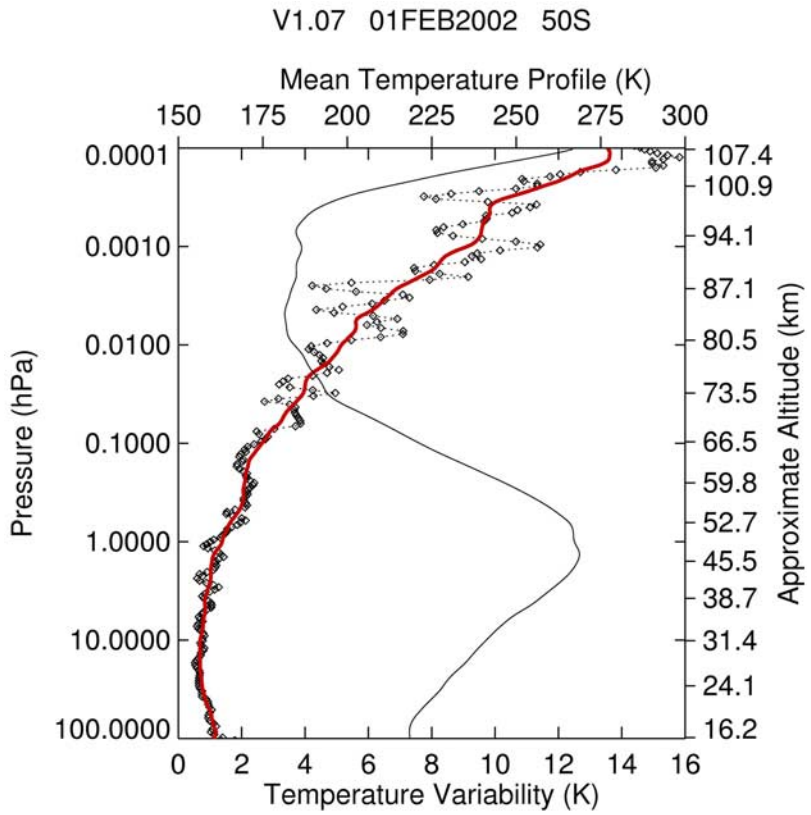

Figure 6. Estimate of precision for the SABER-retrieved $T(p)$, based on the profile of the minimum variability (diamonds) from sets of six consecutive scans from the orbits for 1 February 2002, as they cross the latitude of 50°S. The red curve represents a smoothing of the points in that profile; the associated zonal-mean temperature profile at 50°S is shown (thin curve), so that percentage estimates of the precision can be made.

profiles about their means, as an upper limit estimate of those random variations [see also *Remsberg et al.*, 2003]. Specifically, the dotted curve is the minimum SD profile from among the multiple sets of six successive temperature profiles from the orbital segments crossing near 50°S for 1 February 2002, when $T(p)$ tends to be zonally uniform in the stratosphere and lower mesosphere. The red curve is merely the result of a vertical smoothing of the dotted profile; its variability grows to about 5.5 K at 80 km.

[25] The LTE algorithm iterates on radiances from both channels from 15 hPa to about 1 hPa, from just the radiances of Ch 1 above the 1-hPa level, and from just the radiances of Ch 3 below the 15-hPa level. Forward radiances obtained with the band model approximation for Ch 3 are less than those from the more exact line-by-line (l-b-l) calculations by as much as 0.6% in the upper stratosphere but decrease to half that by 70 km (Figure 5). The exact amount of the difference depends on the atmospheric state giving rise to the radiance profile. The character of the radiance differences for Ch 1 is similar to that of Ch 3. Because the SABER algorithm iterates successively between the radiances of both channels over the range of 15 to 2 hPa used for the determination of pressure altitude, the similarity of the forward model biases for Ch 3 and Ch 1 leads only to small errors for the retrieved $T(p)$. The bias profile for $T(p)$ was obtained by comparing the temperature used for a l-b-l forw diance calculation with the retrieved temperature from the SABER code, wherein its band model radiances were matched against those same l-b-l radiances. The net effect is a radiance bias that is no greater than 0.7% from 15 hPa to 0.1 hPa, as reported in Table 1. Its impact on the retrieved temperatures is no worse than 0.7 K over that pressure range. The simulations indicate small bias errors for $T(p)$ in the lower stratosphere, too. However, those estimates do not include the effects of uncertainties for the retrievals of the co-located, interfering ozone from its Ch 4 radiances; that additional effect is addressed later in this section.

[26] The effect of bias errors in the radiances due to uncertainties in their calibration is considered next in Table 1. At this point it is noted that the temperature uncertainties related to the deconvolution of the instrument FOV function from the radiances are much smaller and are not included separately in Table 1. A nominal, fixed bias of +1% was imposed, in turn, on the radiance profiles of Ch 1 and Ch 3, although that error is considered an upper limit. That radiance error for Ch 1 imparts biases of up to +2 K in the retrieved temperature from about 35 to 60 km, with differences that are smaller both above and below and that become slightly negative below 20 km. A +1% radiance bias for Ch 3 leads to temperature differences of about the same magnitude as those of Ch 1, but of opposite sign. However, the effect of that radiance bias for Ch 3 leads to a change in sign in $T(p)$ at 10 hPa. The effects from Ch 3 are

Table 2. Random and Systematic Errors for SABER Non–Local Thermodynamic Equilibrium T_k for the Upper Mesosphere and Lower Thermosphere for Midlatitude and Polar Summer Cases[a]

	Altitude (km)				
	80	85	90	95	100
		Random			
Noise (one scan)	1.8 (2.7)	2.2 (5.4)	3.6 (8.9)	5.4 (10.3)	6.7 (8.9)
		Systematic			
CO_2 (see text)	1.3	2.8	3.6	3.2	1.4
k_o or [O] by +50%	−0.2 (−0.1)	−0.5 (1.2)	−0.5 (−1.2)	−0.6 (−5.4)	−1.7 (−9.8)
k_o or [O] by −50%	0.3 (−0.3)	1.2 (−1.6)	1.7 (3.8)	1.8 (12.1)	4.7 (23.3)
kvv_min	−0.5 (−4.1)	−0.3 (−5.2)	0.1 (1.6)	0.1 (2.7)	0.1 (2.5)
kvv_max	0.1 (1.2)	0.1 (2.6)	−0.1 (−0.6)	−0.1 (−1.3)	−0.1 (−1.3)
Root-sum-square (±) of random and bias errors	2.3 (5.3)	3.8 (8.2)	5.4 (10.4)	6.5 (16.4)	8.4 (25.8)

[a]Units are kelvins. Polar summer values are given in parentheses.

included in Table 1, in part because they agree closely with some of the differences versus the correlative measurements that we find in section 4. It is also important to note that this positive radiance bias for Ch 3 has an effect equivalent to a 5% increase in the value of p_o. Of course, 1% radiance biases of differing signs are also possible for Ch 1 and Ch 3, but they lead to similar absolute errors in the retrieved $T(p)$ because of the process of iterating between the two channels.

[27] The registration of the SABER radiance profiles with pressure altitude occurs over the range of 2 to 15 hPa. A simple shift of the lower boundary of that region from 15 to 10 hPa leads to temperatures that are higher above the 10-hPa level, but lower below that level; the magnitude of that effect is also given in Table 1. Moving the bottom of that layer downward from, say, 15 to 20 hPa leads to changes of the opposite sign and has an effect similar to that of the +1% radiance bias for Ch 3. The effects of a change of the pressure registration range can come about owing to the differing accuracies for the measured radiances, for their band model approximations, and for the interfering species in Chs 1 and 3. Although a shift from 15 to 10 hPa reduces the sensitivity of the forward model to the uncertainties of the interfering ozone, it introduces additional retrieval instability and occasional spurious event-to-event variations. The upper boundary (2 hPa) of the pressure registration range is affected less by any errors for the interfering ozone. However, that region is still sensitive to uncertainties in the measured radiances; the algorithm depends equally on the radiances of both channels at 40 km, but only on those from Ch 1 at 50 km. The effects of moving that upper boundary are not shown separately in Table 1.

[28] The SABER Level 2 algorithm also performs a concurrent LTE retrieval of the 9.6-μm ozone from the radiances of Ch 4. Those results are particularly sensitive to forward model errors in ozone in the lower stratosphere, where its contributions to the total radiances of Ch 3 are of order 20%. Errors in the corrections for ozone where the pressure registration is performed are also significant but less intuitive because the SABER algorithm performs an iterative fit to the radiances of both Ch 1 and Ch 3 and their percentage contributions from ozone differ. Table 1 shows the effect on $T(p)$ of a 10% underestimate for the retrieved ozone mixing ratio profile. Note that the primary effect is a shift to lower values for the retrieved temperatures somewhat above the 10-hP l and that these lower values persist into the mesosphere. The reason for this behavior is that the primary impact of a bias in the ozone profile is to bring about a change in pressure at the bottom of the registration region. (A 10% overestimate of the ozone leads to a $T(p)$ bias profile of similar magnitude but opposite in sign to that in Table 1.) Further, the LTE retrieval of the Ch 4 radiances leads to excess 9.6-μm ozone in the mesosphere [*Remsberg et al.*, 2007]. Accordingly, the SABER LTE ozone result that is concurrent with the $T(p)$ retrieval is not used above about the 0.4-hPa level; a climatological ozone profile is merged with the LTE ozone values at that point and extended upward to about 0.1 hPa for correcting for its radiance contributions. To summarize, the iterative approach used in the LTE algorithm converges to solutions that may be biased slightly for both $T(p)$ and ozone, and any bias in the retrieved pressure profile affects the registration of the SABER radiances to high in the atmosphere. This outcome points to a potential limitation for obtaining highly accurate determinations of $T(p)$ using a broadband, 15-μm limb radiance technique with only two channels.

3.2. NLTE Algorithm and Uncertainties for T_k

[29] Forward model calculations and the retrieval of T_k from the CO_2 channel radiances are described by *Mertens et al.* [2001] for the UMLT region. In practice, separate NLTE retrievals of T_k were conducted down to 40 km using the radiances of Ch 1, even though they have S/N of no better than 300 at 65 km and 50 at 80 km. Ch 1 rather than Ch 3 radiances were used because the band pass selected for Ch 1 includes fewer of the CO_2 hot bands. Thus, it is easier to model the radiances of Ch 1. Very little radiance smoothing was used for the retrieval of the V1.07 T_k, which accounts for the larger random noise errors for V1.07 values as opposed to those reported by *Mertens et al.* [2001]. The net effect of the noise is given in Table 2 for middle latitude and polar summer cases. For the U.S. Standard Atmosphere T_k profile it is about 1.8 K at 80 km, growing to 3.6 K at 90 km and 6.7 K at 100 km. Errors due to jitter are very secondary to the effects of the noise, so they are not included in Table 2. The effects of noise are larger for the low temperatures near the polar summer mesopause (2.7 K at 80 km to 8.9 K at 90 km and at 100 km). Since the variability of the retrieved results in Figure 6 at 80 to 100 km also includes the effects of the changing atmospheric structure from profile to profile, the values in Table 2 are considered worst-case values for the precision and are larger

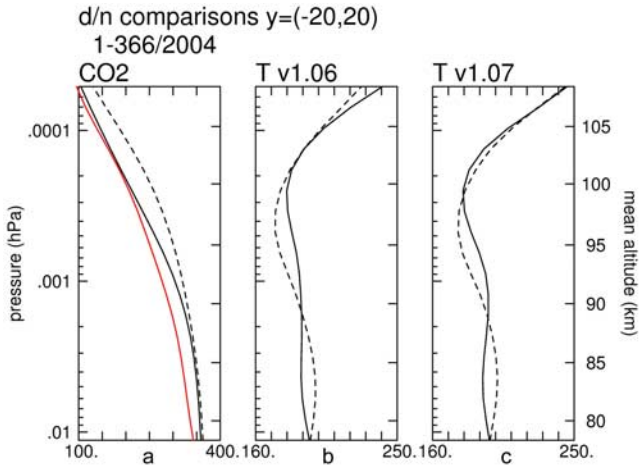

Figure 7. Profiles of (a) CO_2 (ppmv) from V1.06 day (solid black curve), V1.06 night (dashed curve), and V1.07 day and night (red curve); (b) day (solid curve) and night (dashed curve) temperatures (K) from V1.06; and (c) day (solid curve) and night (dashed curve) temperatures (K) from V1.07. Data are averaged for all days in 2004 and for the latitudes between 20°S and 20°N.

than the estimates from just the random noise at middle latitudes.

[30] Principal uncertainties due to bias for the V1.07 NLTE algorithm are also given in Table 2 and are developed in detail for both the middle latitude and polar summer cases in the forthcoming paper of Garcia-Comas et al. (submitted manuscript, 2008). The NLTE band model minus l-b-l radiance profiles differ by +1.0% to +0.5% from 60 to 70 km, respectively, which is the altitude range over which the results from the NLTE and LTE algorithms are merged for V1.07. Even so, the retrieved temperatures differ between the two separate algorithms by no more than ±1 K over that range. The NLTE band model approximation for the radiances improves to less than 0.5% between 80 and 100 km; therefore that source of error is not included in Table 2.

[31] The NLTE retrievals of T_k in the UMLT depend on the knowledge about the decrease of CO_2, and its assumed uncertainties (of up to 15%) according to *Mertens et al.* [2001]. Almost all of the T_k bias at 80 km is due to that source, and their error estimates were adopted for Table 2. At this point the reader is reminded that the V1.04 and V1.06 T_k values were obtained using CO_2 profiles from the TIME-GCM for nighttime, but from SABER-retrieved CO_2 profiles for daytime [*Mertens et al.*, 2008]. In fact, the much larger temperature differences in Figure 2b across all latitudes and above about 90 km are due mainly to those differing CO_2 profiles. The V1.07 NLTE algorithm relies on averages of the day and night CO_2 profiles from the WACCM model after an adjustment that matches them with the CO_2 values used for the LTE algorithm. The use of average profiles from WACCM reduces the uncertainties from the CO_2 itself for the interpretation of diurnal variations in the retrieved SABER temperatures.

[32] Figure 7a shows the tropical, annually averaged zonal-mean CO_2 for three cases: V1.06 day (solid curve), V1.06 night (dashed curve, from TIME-GCM), and V1.07 (red curve, the combined day-night profile from WACCM). Note particularly that there is an offset between the V1.06 day and night profiles that is small at 80 km but becomes larger above 90 km; V1.06 had daytime (retrieved) CO_2 that was lower than its nighttime (specified) CO_2. Its corresponding $T(p)$ profiles in Figure 7b have wavelike, day-night differences due to the diurnal tide but also an offset: $T(p)$ for day being systematically higher than $T(p)$ for night above 90 km. Although the systematic effect in V1.06 is small compared to the short-term tidal variability, it affects the average tidal structure. That offset is eliminated in the V1.07 temperatures (Figure 7c). Furthermore, the TIME-GCM predictions of CO_2 overestimate the observations of CO_2, particularly above 95 km [*Lopez-Puertas et al.*, 2000; *Kaufmann et al.*, 2002; *Mertens et al.*, 2008]; the V1.07 values from WACCM are closer to those same observations (not shown).

[33] T_k depends on the knowledge of the increase of [O] with altitude in the UMLT [*Mertens et al.*, 2001]. The V1.07 and V1.06 profiles of [O] were inferred as part of the SABER retrievals of the 1.27-μm channel radiances for ozone, at least below 95 km for daytime (defined as having a SZA of less than 85 degrees). Nighttime and twilight profiles of [O] and its daytime values above 95 km were obtained for V1.07 from the NRL-MSISE-00 model [*Picone et al.*, 2002]. For daytime the model [O] was shifted to match the retrieved [O] at 90 km, and then those values were merged from 90 to 95 km.

[34] T_k also depends on the rate for the physical quenching of $CO_2(\upsilon)$ with [O], taken as $3.5 \times 10^{-13} \sqrt{T} + 2.3 \times 10^{-9} \exp(-76.5/T^{1/3})$ $cm^{-3}s^{-1}$ in the SABER operational algorithm [*Sharma and Wintersteiner*, 1990]. Laboratory studies indicate a slower rate for this quenching reaction. Therefore the [O] is uncertain by at least ±50%, while the $CO_2(\upsilon_2)$-O quenching rate has only a negative uncertainty since its upper limit is already being used in the operational algorithm. Slower rates and/or smaller values of [O] lead to higher retrieved values of T_k and have the larger uncertainties for altitudes above about 85 km. Simulations were conducted for cases where either the rate constant k_o or the value of [O] was changed by −50% or by +50% (Garcia-Comas et al., submitted manuscript, 2008). Results of those simulations are given in Table 2. At altitudes greater than 100 km the uncertainty due to the CO_2 (υ_2) quenching mechanism dominates all the other systematic errors. The T_k errors due to uncertainties in the non-LTE constants depend on latitude and season. Additionally, there are uncertainties in T_k from the rate of $CO_2(\upsilon_2)$ vibrational quanta exchange. The rates used in V1.07 for those processes lie within the available laboratory measurements, that is, kvv_min = 1.2e − 11 and kvv_max = 2.4e − 11 cm^3 s^{-1} (see the work of Garcia-Comas et al. (submitted manuscript, 2008) for details). Those error estimates are small for the middle latitudes but much larger for polar summer (Table 2).

[35] To summarize, the combined effects of the uncertainties for a single LTE $T(p)$ profile are given in Table 1: its root-sum-square (RSS) values. The corresponding non-LTE RSS uncertainties for T_k are in Table 2. They vary from ±8.4 K at 100 km to ±3.8 K at 85 km for the middle latitudes, and they compare very favorably with the estimates of accuracy for T_k from the Cryogenic Infrared Spectrometers

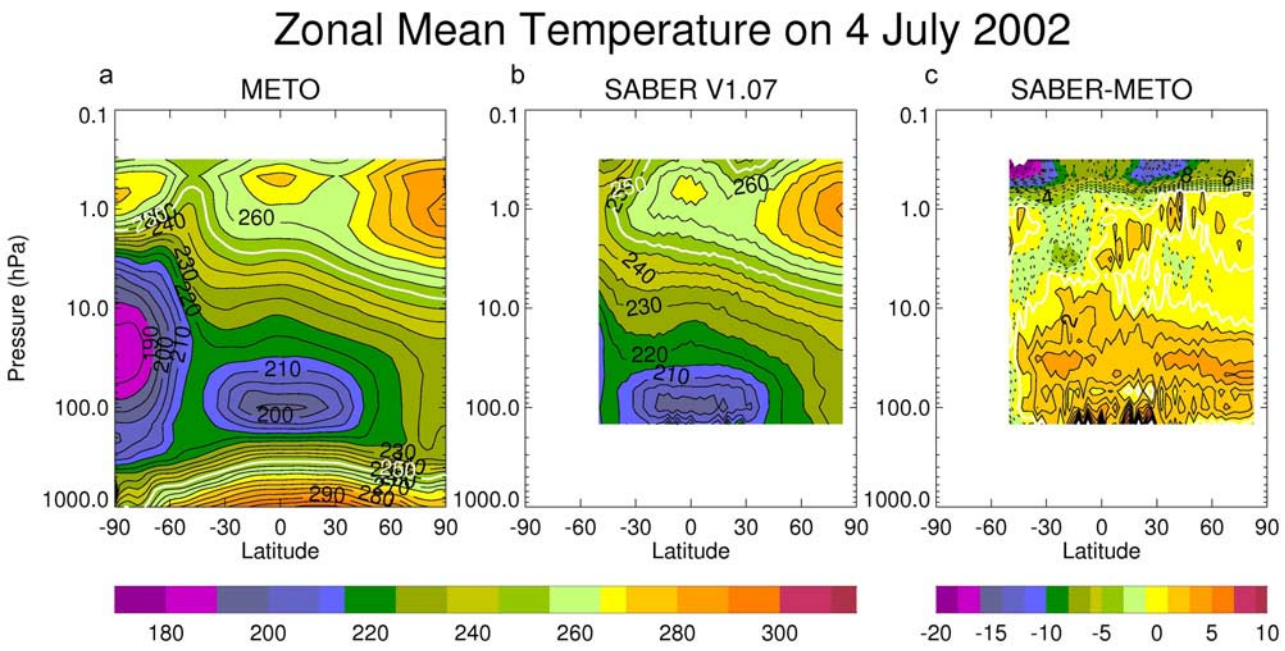

Figure 8. (a–c) Comparison of the zonally averaged SABER V1.07 $T(p)$ with the results from the operational analyses of the U.K. Met Office (MetO) for 4 July 2002. Figure 8c shows the zonal-mean plot of the differences (K), SABER minus MetO, where the dashed curves and the solid curves are the negative and positive contours, respectively. Contour increment for the differences is 1 K.

and Telescopes for the Atmosphere (CRISTA) instrument [*Gusev et al.*, 2006]. The SABER T_k uncertainties range from ±25.8 K at 100 km to ±8.2 K at 85 km for polar summer. The goal of sections 4 and 5 is to verify the estimates of accuracy by comparisons with other well-characterized data sets.

4. Quality of SABER $T(p)$ and Heights for the Stratosphere and Mesosphere

4.1. Comparisons With MetO Analyses and With Rayleigh Lidar Profiles

[36] Previously, *Remsberg et al.* [2003] reported on the data precision and accuracy for the SABER V1.01 $T(p)$ and geopotential heights. Qualitatively, the findings about V1.07 and V1.06 $T(p)$ are nearly identical to each other and are similar to those of V1.01, at least for the stratosphere and lower mesosphere. Figure 8 shows the zonally averaged temperatures from the U. K. Met Office (MetO) analyses and SABER V1.07 and their differences for 4 July 2002. SABER temperatures are higher by several degrees at most latitudes below about the 15-hPa level, due most likely to slight biases in the radiances for Ch 3 or from its band model and its interfering ozone. In the upper stratosphere the SABER temperatures are lower than those of MetO by a degree or so, although that small bias is within the accuracy for the MetO $T(p)$ at those levels [*Randel et al.*, 2004; *Manney et al.*, 2005; *Shine et al.*, 2008]. It is also noted that the MetO values for the lower mesosphere are essentially based on an extrapolation from the upper stratosphere; differences at those higher altitudes are not considered significant. Positive temperature differences for the lower stratosphere and negative differences for the upper stratosphere are also characteristic of the effect of a positive radiance bias for Ch 3 (Table 1).

[37] The comparison differences in Figure 8c also indicate that there is little to no temperature bias in the SABER data in the uppermost stratosphere at high northern latitudes in early July. SABER views to the north and in the direction of the positive temperature gradient of the summertime stratopause at that time (see Figures 8a and 8b) for both its ascending and descending orbital segments. There are also significant meridional gradients in $T(p)$ for the middle to upper stratosphere from 30°S to 60°S in Figure 8c, where SABER is lower than MetO. Biases due to not correcting for such gradients, while small, will depend on the viewing direction and atmospheric state. It is noted that such gradient corrections were applied to the LIMS V6 data set. They were determined to first order from the daily mapped analyses of its earlier V5 product and then applied to the LOS state vectors for the retrievals of the scans of V6. A similar approach could be used for a reprocessing of the SABER data set, if necessary.

[38] SABER V1.01 did not contain geopotential height as a profile product; it was obtained by generating maps of the thickness fields from SABER and then adding their gridded values to the heights of the MetO analyzed fields at 100 hPa. That approach was changed for Versions 1.06 and 1.07; their height profiles were generated for the Level 2a files, as follows. Initially, a relative altitude profile was obtained from the ephemeris information for the spacecraft pointing. Any offset in relative altitude was determined by comparing the SABER altitude at 10 hPa with the corresponding altitude of the 10-hPa surface from the objective analyses

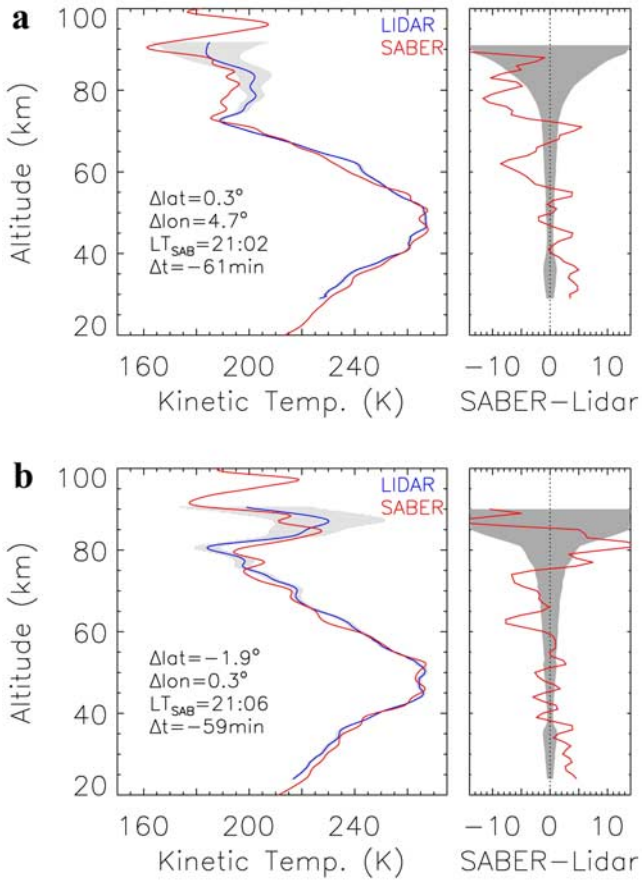

Figure 9. (a) SABER V1.07 $T(z)$ profile (red curve) compared with a Rayleigh lidar sounding (blue curve) at Table Mountain, California, for 8 June 2002. Right profile shows SABER minus lidar result (in K); shading in the vertical represents the combination of random and systematic errors from the lidar measurement. Average time difference is 61 min for the two soundings. (b) As in Figure 9a but for 9 October 2002. Average time difference is 59 min.

of the National Centers for Environmental Prediction (NCEP). In other words, the SABER relative altitudes were adjusted on the basis of a match of the NCEP and the SABER-derived pressures. Then, the profiles of geopotential height were obtained by applying the integral of g(z) dz, where g(z) is gravity and z is the altitude. Zonally averaged, SABER geopotential heights versus latitude were compared with those from the MetO for the test day, 4 July 2002 (not shown). Those SABER minus MetO results are negative in the lower stratosphere (by as much as −100 m at 100 hPa), are near zero at about 30 hPa, are +50 m at 15 hPa (or near p_o), and become larger at higher altitudes (by up to 200 m at 1 hPa). It is also noted that the MetO heights are lower than those of NCEP by 100 to 150 m at 10 hPa across most latitudes for that day: a measure of the uncertainties for those two comparison data sets.

[39] Quite a few coincident comparisons were obtained with Rayleigh lidar measurements at two NDACC (http://www.ndsc.ncep.noaa.gov/data) sites: Mauna Loa, HI, (20°N) and Table Mountain, CA, (34°N) in 2002 through 2005. The coincidence criteria are within 2 degrees of latitude, 5 degrees of longitude, and 2 hours in time. There were also several coincidences over Sondre Stromfjord, Greenland (67°N) for 2 ll the comparisons were made in terms of $T(z)$ because that is the natural retrieved product from a lidar backscatter measurement. The lidar profiles are based on measurements obtained over periods of about 1.5 hours and have an effective vertical resolution of 1 to 2+ km from 10 to 65 km and 2 to 4 km from 65 to 80 km, or similar to that of the SABER results [*LeBlanc et al.*, 1998]. Lidar resolution degrades to 7 km at 90 km—a result of the need to average its weaker return signals. An estimate of $T(z)$ precision for the lidar profiles is obtained from the statistics of the shot noise for the laser source. That precision is of order ±5 K at 80 km but smaller than ±1 K at 55 km and below.

[40] Two comparison examples are given for the Table Mountain site. Figure 9a shows coincident profiles from 8 June 2002, and Figure 9b is a profile pair from 9 October 2002. Their associated SABER minus lidar differences are shown in the right profiles for each pair along with the total error (shading) for the lidar data. These two examples were selected because of their lack of substantial vertical structure in the stratosphere and the lower mesosphere (below about 70 km), making it easier to check for any effects of a profile registration bias for the SABER profile. Vertical features of the comparison profiles agree closely with those of SABER, nonetheless. Most noteworthy, their respective

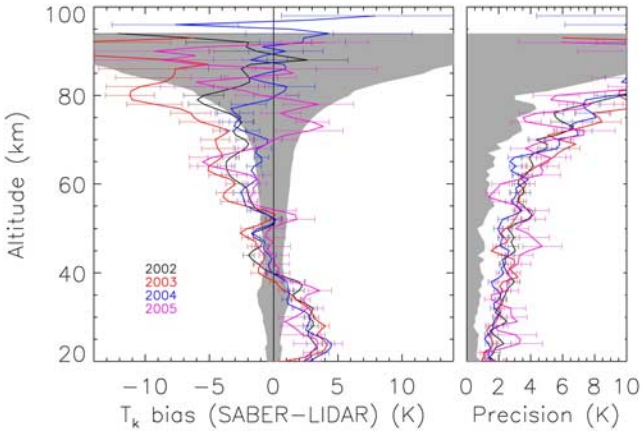

Figure 10. Profile of the average temperature differences, SABER minus Rayleigh lidar, from the sets of profile pairs at Table Mountain for 2002 (39 pairs), 2003 (25 pairs), 2004 (28 pairs), and 2005 (8 pairs). Shaded region is the combined random and systematic error for the lidar data. The average variability of the paired differences for each year is to the right, along with the estimated precision for the SABER profiles (shaded).

temperature structures agree well in the upper mesosphere, where the temporal scales for the vertical waves are short. At Mauna Loa the effects of the propagating tides are present in the SABER $T(z)$, and their phases also agree with the vertical structure in the lidar profiles (not shown).

[41] Figure 10 contains four yearly averages (2002–2005) of the SABER minus lidar results and of their standard deviations for the Table Mountain site. The number of comparisons for each year is 39, 25, 28, and 8, respectively, although fewer of the lidar profiles extend to the highest and lowest altitudes. The combined systematic and random errors for the lidar profiles are shaded; similar estimates for SABER are given at the bottom of Tables 1 and 2. The estimate of the precision for the differences is shown in the right profile, along with an estimate of the precision of the SABER data that was determined in the same manner as for Figure 6. These differences do not change significantly when the spatial and temporal coincidence criteria are reduced. The biases between the average profiles are similar for each year, except in the upper mesosphere. SABER minus lidar $T(z)$ is positive (warmer by 2 to 4 K) below 40 km, changes noticeably from positive to negative near 40 km, and is negative (cooler by 1–3 K) from about 40 to 60 km. Biases that change from positive to negative at about 40 km (near 3 hPa) and become more negative with altitude are characteristic of a bias error in the radiances of Ch 3 combined with a changeover from relying on both Ch 3 and Ch 1 radiances at 40 km to relying on just the Ch 1 radiances at 50 km. From 60 to 80 km the SABER minus lidar values are mostly negative, though much more variable. Separate sets of comparisons indicate that there is no clear seasonal dependence to these results (not shown).

[42] The average bias profile versus the Mauna Loa data is shown in Figure 11 and has a similar pattern to that of Figure 10 below about 70 km; however, the differences at Mauna Loa are generally smaller by 1 K or SABER warmer than lidar by only 1–3 low 40 km. Above 80 km the SABER temperatures are greater than from the lidar. The bias profile at Sondre Stromfjord (not shown) is also similar to those of the other two stations from about 45 to 70 km, but than SABER $T(p)$ is less than from lidar by 2 to 4 K from 30 to 40 km.

[43] *Remsberg et al.* [2002] conducted similar comparison studies for HALOE temperature profiles versus those obtained with the Rayleigh lidar at the OHP station in France and with falling spheres from several rocket sounding locations. They found that the HALOE profiles also had a low bias versus lidar that increased from 60 to 80 km, but that HALOE had no similar persistent bias versus the falling sphere profiles. On the basis of their additional HALOE comparisons with profiles obtained from a shipboard lidar of higher laser power and thus having a higher starting altitude for its profiles, they concluded that the OHP lidar profiles had a systematic high bias in the uppermost mesosphere. That bias was ascribed to errors in the subtraction of background signals for the Rayleigh lidar measurements of the upper mesosphere. Similar biases may be affecting the SABER comparisons with lidar in Figures 10 and 11, but they are not included in the estimates of accuracy for the lidar results at the Table Mountain and Mauna Loa sites. Therefore the apparent SABER biases with Rayleigh lidar in the upper mesosphere may not be so significant.

[44] To summarize this section, the SABER stratospheric temperature and geopotential height distributions compare well with those from the MetO analyses for a test day. SABER V1.07 and V1.06 $T(p)$ is higher by 2 to 3 K in the lower stratosphere (20 to 50 hPa) and lower by 1 to 2 K in the upper stratosphere, although the latter differences are within the uncertainties of the MetO analyses. SABER values are also higher than the lidar data below about 40 km by 1 to 3 K. Such systematic differences in $T(z)$ for the lower stratosphere are somewhat larger than estimated in Table 1. However, this high bias for SABER is consistent with the fact that the SABER ozone is less than that from MIPAS at about 21 km (near 40 hPa): an expected result if the associated SABER temperatures are too high for the retrieval of the 9.6-μm ozone from its infrared limb radiances (P. P. Rong et al., Validation of TIMED/SABER v1.07 ozone at 9.6 μm in altitude range 15–70 km,

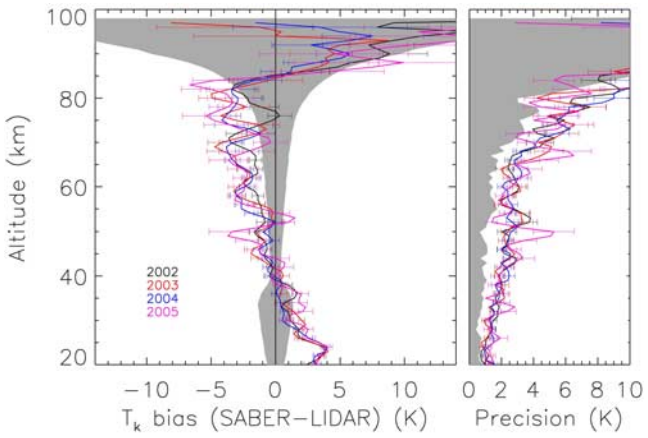

Figure 11. As in Figure 10 but for the Rayleigh lidar at Mauna Loa.

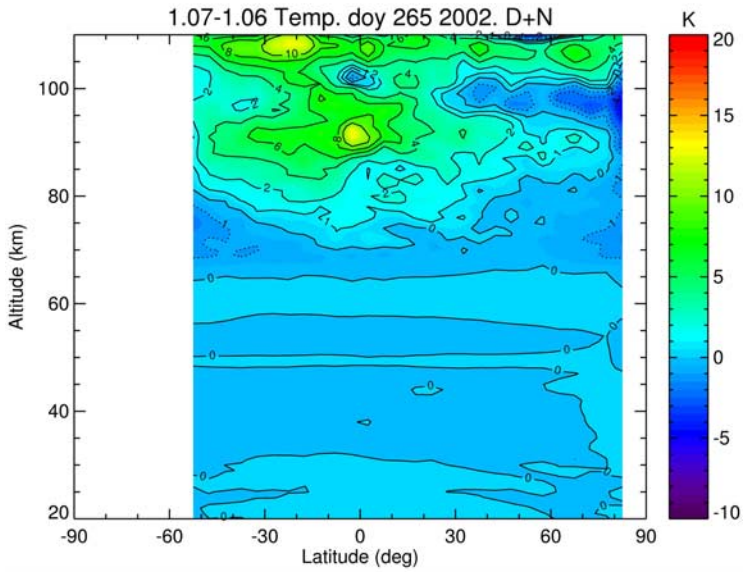

Figure 12. Zonally averaged SABER temperature differences, V1.07 minus V1.06, for 22 September 2002. Contour increment is 1 K; negative contours are dashed.

submitted to *Journal of Geophysical Research*, 2008). SABER $T(z)$ is lower than lidar by 1 to 3 K from about 40 km and into the lower mesosphere. This finding is consistent with an underprediction of the 4.3-μm (SABER Ch 7) radiances, as obtained using the SABER $T(z)$ profiles [*Lopez-Puertas et al.*, 2004]. SABER differences versus lidar are not of the same sign for the Mauna Loa versus the Table Mountain data sets for the upper mesosphere.

4.2. $T(p)$ Comparisons With MLS and ACE

[45] The AURA Microwave Limb Sounder (MLS) V2.2 [*Schwartz et al.*, 2008] and the SCISAT-1 Atmospheric Chemistry Experiment (ACE) V2.2 [*Sica et al.*, 2008] data sets for $T(p)$ were compared with the SABER V1.06 results in the stratosphere and mesosphere. Although the present study does not include additional MLS or ACE comparisons, a review of their findings is given here. For the MLS comparisons, *Schwartz et al.* [2008] made an accommodation for the differing vertical resolution of the SABER profiles in the stratosphere and lower mesosphere, but not for higher altitudes. They found that SABER is higher than MLS by 2–3 K in the lower stratosphere, has no clear bias in the upper stratosphere, is lower by 3–5 K at the stratopause, but then is higher again by 3–5 K in the lower mesosphere. They reported no apparent problems for the registration of the SABER or MLS profiles. The comparisons with ACE of *Sica et al.* [2008] were necessarily limited to its measurements at sunrise (SR) and sunset (SS). They found small differences for several sets of comparisons; SABER temperatures were higher than ACE by 2 K near 23 km, but lower by 2–3 K above 50 km. Thus, their comparisons gave findings that are similar to those of SABER versus MetO and the Rayleigh lidar, as shown in section 4.1.

[46] *Manney et al.* [2008a, 2008b] used SABER V1.06 temperatures to characterize the dynamics associated with the NH polar stratopause during stratospheric sudden warming (SSW) events. In p r, they found that the SABER profiles were changing in the same way as the co-located measurements from MLS, ACE, and the Rayleigh lidar profiles at Eureka, Canada (80°N, 274°E) during those dynamically disturbed events. Where differences occurred, they were attributed primarily to the differing viewing directions for the separate measurements. However, *Manney et al.* [2008b] found that SABER/MLS agreed less well with the Goddard Earth Observing System (GEOS) Version 5.0.1 operational analyses during and especially after the SSW events because of failings of the analyses themselves.

[47] The SABER V1.07 minus V1.06 temperature distribution was shown in Figure 2b for a daytime orbital segment of the Northern Hemisphere just following summer solstice, and its differences are near zero below about 70 km even at the midlatitudes to high latitudes. Figure 12 shows the V1.07 minus V1.06 zonally averaged differences at equinox, 22 September 2002. Those differences are of order 1 K or less below about 75 km. Therefore the findings of the comparisons with SABER in the works of *Schwartz et al.* [2008], *Sica et al.* [2008], and *Manney et al.* [2008a, 2008b] should not change below about 70 to 75 km for V1.07.

4.3. Comparisons With MIPAS and HALOE

[48] In the following paragraphs, SABER comparisons with the MIPAS and then the HALOE data sets are reported. Both comparison data sets extend across most latitudes, have vertical resolutions that are similar to that of SABER, and are well characterized, at least below 68 km. MIPAS was launched on Envisat into a polar orbit on 1 March 2002, and it obtained measurements at two local times of the day. *Ridolfi et al.* [2007] reported on the quality of the MIPAS temperatures, which extend from 6 to 68 km. Its limb scans were obtained with vertical steps of 3 km from 6 to 42 km and of 5 to 8 km above 42 km. The MIPAS profiles are from an LTE algorithm, and their retrievals were conducted for radiances from spectral lines that are resolved well with its Fourier Transform Spectrometer. In this regard its radiances have narrow vertical weighting functions that are confined

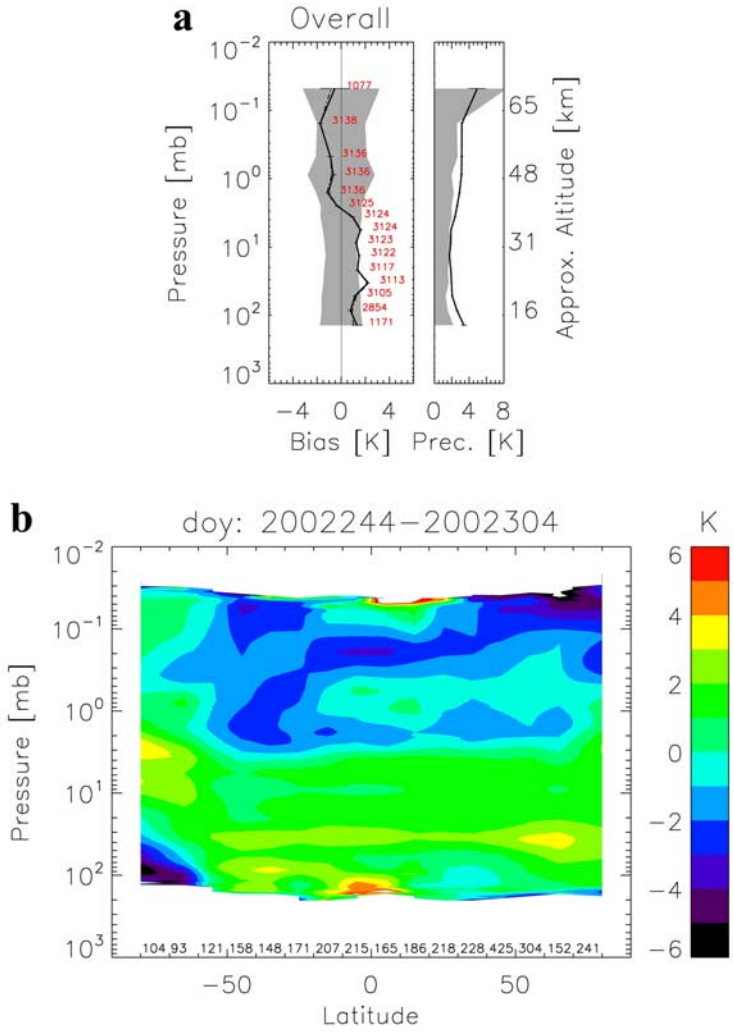

Figure 13. (a) SABER minus Michelson Interferometer for Passive Atmospheric Sounding (MIPAS) temperature differences based on their coincidences in September–October 2002. The left profile shows mean differences as calculated from all the latitude boxes having a width of 10 degrees; the number of pairings is given in red, and the shading is the combined systematic errors for SABER and MIPAS. The right profile is the average variability or SD of the differences, while the shading is the combined SABER and MIPAS random errors. (b) Zonal average distribution of the SABER minus MIPAS temperature biases (in K). Numbers of colocated pairs are along the bottom, as averaged for each latitude bin.

more closely to its tangent layers than is the case for the broadband CO_2 channels of SABER, especially for the upper stratosphere and the mesosphere. *Ridolfi et al.* [2007] note that comparisons with correlative measurements in terms of $T(p)$ are likely more accurate than in terms of $T(z)$, because of their dependence on a reference height from an operational analysis product for the conversion of pressure to geometric altitude. They found agreement for $T(p)$ to within 1 to 2 K with balloon-borne correlative measurements for the altitude range of 6 to 36 km. Their MIPAS minus lidar results were obtained in terms of $T(z)$, but with an adjustment of the MIPAS altitudes according to how different they were from those of nearby radiosonde soundings. In almost all cases MIPAS agreed with the lidar data to within ±2 K from 30 to 70 km, although with a noticeable change in sign for the low and middle latitudes near 42 km: positive below to negative above. At high latitudes the character of those differences was reversed, however.

[49] Comparisons are shown herein between SABER V1.07 and the MIPAS ESA operational (V4.61 and v4.62) $T(p)$ data for July through December 2002. A large number of co-located pairs were obtained; they are within 2 deg in latitude, 5 deg in longitude, and a maximum of 2 hours in time. Then their mean profiles were calculated for 10-degree-wide latitude zones, as well as for their global mean differences. The zonally averaged, SABER minus MIPAS result for the 60-day equinox period of September–October spanning parts of two yaw cycles (days 244–304) is shown in Figure 13a; results were also obtained for the other seasons, and they are similar (not shown). Figure 13a (left profile) shows the global mean difference profile, which is composed of about 3000 sample pairings (in red). The shaded area is the combined, estimated systematic errors

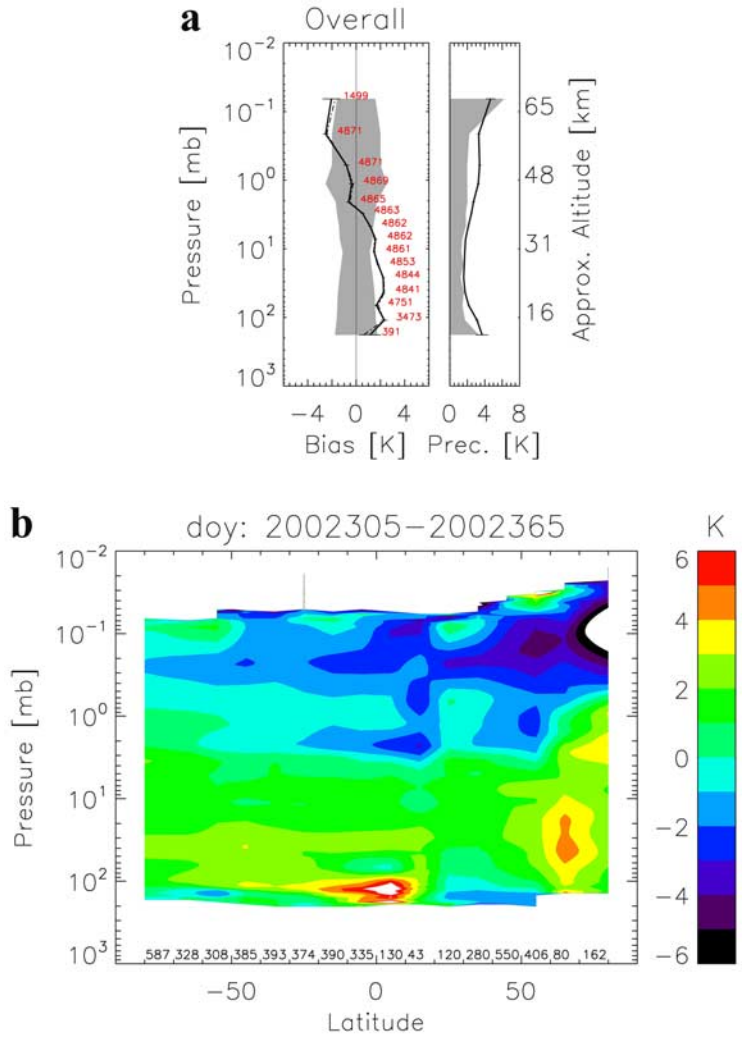

Figure 14. (a) As in Figure 13a but for November–December 2002. (b) As in Figure 13b but for November–December 2002.

for MIPAS (see http://www.atm.ox.ac.uk/group/mipas/err/) and from Table 1 for SABER. Specifically, that shading represents the root-sum-square (RSS) of those MIPAS and SABER systematic errors. The horizontal bars on the profile are the estimated uncertainties for the mean difference profile. The standard deviation of the differences and the estimated SABER plus MIPAS random errors (shaded) are shown in the right profile. An approximate mean geometric altitude for the SABER average profile is given on the ordinate of Figure 13a (right profile).

[50] Figure 13b is the corresponding latitude-pressure contour plot of the mean differences for that equinox period. It indicates that SABER $T(p)$ is systematically higher by 1–2 K below about the 3-hPa level, but lower by about 1–2 K above that. There is a pronounced band of positive differences at about 40 hPa but a band of negative differences at 2 hPa, extending across almost all latitudes. It is noted that the changeover from a positive bias to a negative bias occurs near the top of the pressure-altitude range that is used for the registration of the SABER profiles. The shapes and magnitudes of the profile differences are also similar to those reported from the SABER/ACE, SABER/MetO, and SABER/lidar comparisons. Differences of order −3 to −4 K occur at middle latitudes near 0.1 hPa, and on inspection one can see hints of similar differences in the individual lidar comparisons between 60 and 65 km of Figures 9a and 9b. The pattern of the negative differences in the midmesosphere in Figure 13b varies somewhat with latitude, possibly related to how well vertical structures in the radiance profiles are being resolved. This region of 60 to 70 km is also where the outputs from the SABER LTE and NLTE algorithms were merged, although their separate results tend to agree to within about ±1 K. For the MIPAS retrievals the altitude of 68 km is the midpoint of the first layer below its top boundary; thus, there can be larger biases for the temperature of that first layer.

[51] Figures 14a and 14b show the SABER minus MIPAS results for the solstice period of November–December 2002 spanning parts of two yaw cycles (days 305–365), and its differences have nearly the same pattern as those of Figures 13a and 13b. Note that the persistent positive bias near 40 hPa is shifted more toward the Southern Hemisphere, while the negative bias in the middle mesosphere is more pronounced in the Northern Hemisphere. There is less

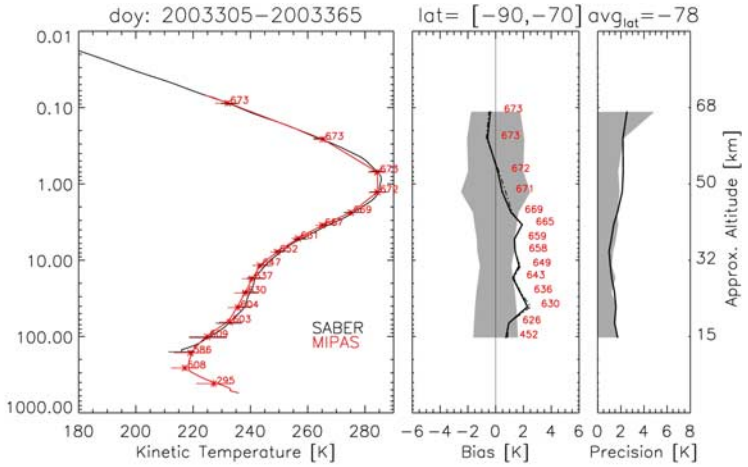

Figure 15. SABER/MIPAS temperature comparisons for the period November–December 2003 and for the latitude bin of 70°S–90°S. (left) Comparison of their average profile. (middle) Average bias profile from the paired differences, SABER minus MIPAS, with shading and number of pairs as defined in Figure 13a. (right) Average variability of SD of the differences with shading as defined in Figure 13a.

evidence for a persistent negative bias across all latitudes near 2 hPa. There are positive anomalies for the differences at 3 hPa near 70°S in Figure 13b and at 40 hPa at 65°N in Figure 14b, possibly owing to not accounting for the effects of horizontal temperature gradients in the forward radiance calculations along the limb-viewing paths for SABER or MIPAS (or both) near the edge of the vortex.

[52] There is a negative anomaly for the differences in Figure 13b in the lower stratosphere at 70–80°S, where the SABER scans were taken looking south from 7–19 September. That anomaly may be due, in part, to not accounting for the effects of polar stratospheric clouds (PSC) in the forward model for Ch 3; the temperature anomaly due to PSCs is estimated to be no greater than about 2 K, however. As a further indication of quality of the SABER profiles at high latitude, Figure 15 shows the average differences for over 600 pairs at high southern latitudes in late autumn/early summer (November–December) 2003 and at a time when the PSCs were dissipated. Note that the average SABER biases are no greater than +2 K in the stratosphere or −1 K in the mesosphere at this time, which is well within the combined errors for the two data sets. In the upper mesosphere the polar mesospheric clouds (PMC) begin to form just above the 0.01-hPa level in December. However, no indications of PMC signatures have been found in the Ch 1 radiances that are used for the retrievals of the SABER temperatures at those altitudes.

[53] The HALOE experiment operated on the UARS satellite from October 1991 through November 2005 [*Russell et al.*, 1993]. Its algorithms provide unique $T(p)$ profiles from about the 4-hPa level to near the 0.005-hPa level and with vertical resolutions of 3 to 4 km, or somewhat broader than those of SABER [*Hervig et al.*, 1996; *Remsberg et al.*, 2002]. Previous comparisons with correlative lidar and falling sphere measurements indicate that the HALOE V19 profiles are accurate to within 3 K from 33 to 66 km and within 4 K to 74 km [*Remsberg et al.*, 2002]. The HALOE $T(p)$ values were extended below the 4-hPa level by a merger with the NOAA/Climate Prediction Center (CPC) analyses bove the 0.004-hPa level with ties to the MSIS model profiles. However, a recurring issue for comparisons with solar occultation measurements is that coincidences are few on any given day, and often not very close in longitude or local time. Thus, it is expected that there will be differences for the vertical structure of the paired profiles, especially for the mesosphere. The approach used herein is to consider zonal average comparisons when the HALOE sunrise (SR) and sunset (SS) profiles were at nearly the same latitude, its so-called "latitude crossover occurrences." At low and middle latitudes those SR and SS measurements are nearly 12 hours apart.

[54] For example, SABER/HALOE comparisons were obtained for the latitude band of 15 ± 5°S on 7–8 June 2002. There are a total of 28 SR and 30 SS HALOE profiles across those two days. The corresponding SABER ascending profiles occurred at about a 90 degree solar zenith angle (SZA) and were very close to the local time of HALOE SR. The SABER descending profiles were taken at SZA near 155 degrees on these two days or about 3 hours after HALOE SS. The zonally averaged values for the sets of SABER ascending and HALOE SR profiles are shown in Figure 16a. The average SABER profile is several degrees colder than that of HALOE in the upper stratosphere and lower mesosphere, although within their combined accuracies. Average values for the SABER descending and HALOE SS profiles are shown in Figure 16b. In this case their agreement is even better. In both cases the SABER and HALOE profiles tend to diverge above the 0.005-hPa level, where the WACCM CO_2 of the SABER algorithm is beginning to decrease and where the MSIS temperature model is being merged with the retrieved HALOE $T(p)$.

[55] Figure 17a shows the respective SABER minus HALOE differences for the comparisons of their zonal means of Figure 16. The vertical oscillations in those differences are primarily because the SABER measurements have better vertical resolution and sensitivity than those of HALOE. The horizontal bars of the solid profile are the RSS of the systematic errors for SABER and HALOE, and the differences are within those uncertainties up to about the 0.01-hPa level. The same error bars can be applied to the

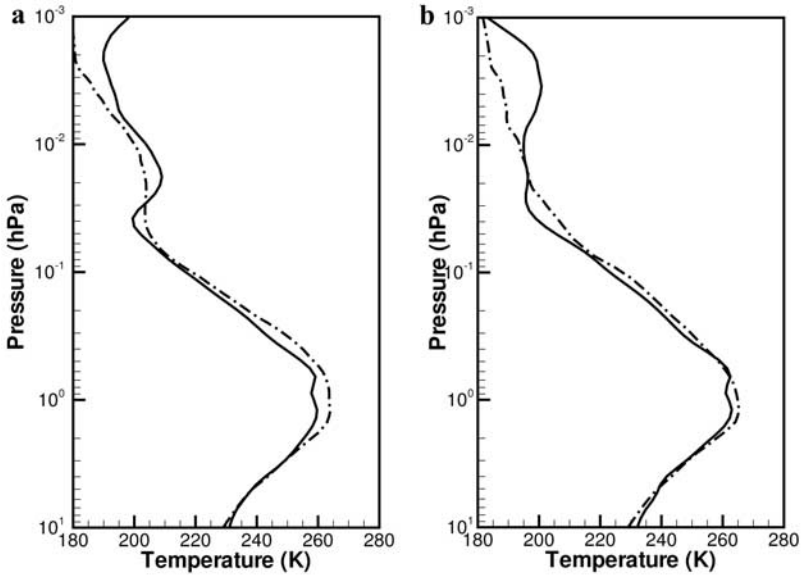

Figure 16. Zonally averaged SABER (solid curve) and Halogen Occultation Experiment (HALOE; dash-dotted curve) temperature profiles for 10°S–20°S on 7–8 June 2002. (a) SABER ascending, HALOE sunrise (SR). (b) SABER descending, HALOE sunset (SS).

dashed curve. In general, the SABER values are lower than those of HALOE from the upper stratosphere to about the 0.04-hPa level, most noticeably for the SABER ascending minus HALOE SR differences (Figure 17a, solid curve) that had a very good time-of-day coincidence. Those negative differences vary from about −2 to −5 K, and the magnitude and the altitude region for the biases agree generally with those from the SABER comparisons with MIPAS and with the Rayleigh lidar. Above about the 0.02-hPa level the differences are clearly positive for the SABER ascending versus HALOE SR profile (Figure 17a, solid curve). The SABER descending minus HALOE SS average profile (Figure 17a, dashed curve) becomes clearly positive above about the 0.007-hPa level. Biases above the 0.004-hPa level are likely a result of the HALOE merger with the MSIS climatology.

[56] Figure 17b shows the average SABER ascending minus descending profile (solid curve) and the average HALOE SR minus SS profile (dashed curve). One can clearly see the effects of the tidal oscillations in both of them. The respective tidal amplitudes increase with pressure altitude, and their apparent vertical wavelengths are similar. The somewhat larger amplitude of the tide from SABER is indicative of the better vertical resolution of its measurements. The phases of the oscillations for the average profiles disagree near 0.5 hPa, possibly owing to the fact that the

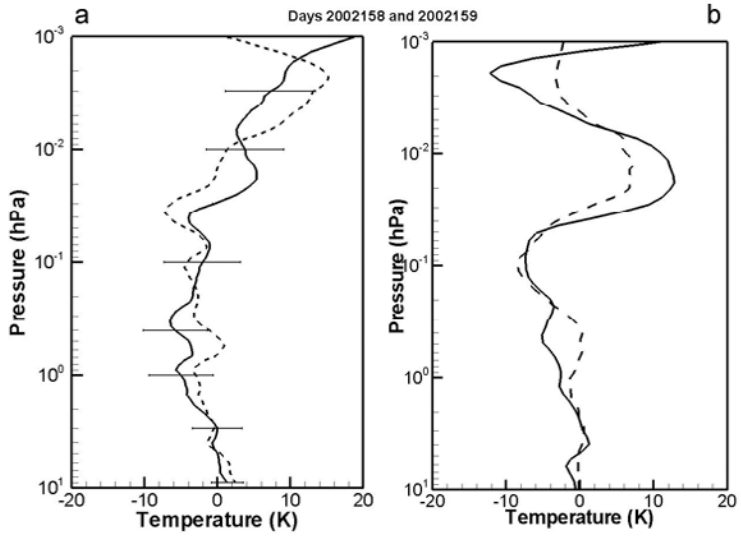

Figure 17. Profile comparison of temperature differences (in K). (a) SABER ascending minus HALOE SR (solid curve) and SABER descending minus HALOE SS (dashed curve); horizontal bars are the root-sum-square (RSS) systematic errors from SABER and HALOE. (b) SABER ascending minus descending (solid curve) a LOE SR minus SS (dashed curve).

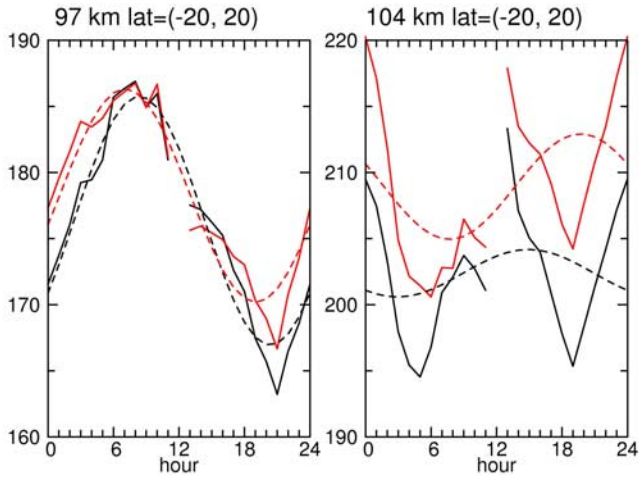

Figure 18. Diurnal variation of temperature (K) for low latitudes at (left) 97 km and (right) 104 km. Solid curves are temperature in local time bins from V1.06 (black) and V1.07 (red). Dashed curves are least squares fits to those SABER data. Data are averaged for all days in 2004 and for latitudes between 20°S and 20°N.

SABER ascending and descending profiles were apart by 9 hours rather than 12 hours. Note also that the tidal amplitudes for HALOE (Figure 17b, dashed curve) at its highest altitudes become nearly zero because of its merger with the MSIS profile; SABER provides a more realistic tidal signature for the UMLT region (see also section 5).

[57] It is most often the case that the HALOE SR and SS profiles were taken when neither the SABER ascending nor descending profiles were close to a 90 degree SZA. In other words, the HALOE SR and SS profiles were nearly 12 hours apart, but the associated SABER profiles differed from them in local time by at least several hours. This circumstance occurred for a HALOE SR/SS crossover at Southern Hemisphere middle latitudes on 28 March 2002. In that case (not shown) the SABER descending (daytime) and the HALOE SR zonal averages were within the latitude range of 28°S to 36°S but only 8 hours apart; even so, the differences for their means are very near zero from 4 hPa to 0.01 hPa. On the other hand, the SABER ascending (nighttime) minus the HALOE SS zonal averages for that day were within the latitude range of 36°S to 42°S and 6 hours apart. That comparison shows differences varying from +12 K to −7 K through the upper mesosphere, indicating that there were significant effects at those latitudes due to variations from atmospheric planetary and/or gravity waves. Seldom did we find SABER and HALOE profiles that had a very close, time-of-day coincidence. Thus, it is difficult to obtain a large set of coincident SABER and HALOE profiles for making better judgments about the accuracy of the SABER temperatures in the mesosphere.

5. Quality of the SABER Temperatures in the UMLT Region

5.1. Tidal Signatures

[58] In this section the signature of the temperature tide from V1.07 is checked first. Following that, SABER comparisons with corre measurements for two Northern Hemisphere midlatitude sites are shown for the UMLT to see whether V1.07 T_k is being provided to the accuracies in Table 2. Comparisons are considered with the column-averaged temperatures based on the measured emissions from the separate OH and O_2 layers for the ground-based station at Granada, Spain (37°N, 357°E) [*Lopez-Gonzalez et al.*, 2007] and for the ground-based station at Maui, Hawaii (25°N, 204°E) [*Taylor et al.*, 2005]. Then, comparisons are shown versus the $T(z)$ profiles obtained with the sodium (Na) lidar at Fort Collins, CO (41°N, 255°E) [*She et al.*, 2004]. Finally, we consider the quality of the temperatures from the SABER algorithm for daytime by showing comparisons with the falling sphere climatology of *Lübken* [1999] in the region of the polar summer mesopause.

[59] As pointed out in section 3.2 and Figure 7, the V1.07 algorithm uses specified CO_2 that has no day-night difference. This approach is a change from that used for V1.06, where its daytime CO_2 was retrieved but its nighttime values were specified from TIME-GCM. To illustrate the impact that the day-night offset can have on a tidal analysis with the V1.06 data, Figure 18 shows 2004 temperatures binned in local time for the tropical region along with diurnal fits to those data. The analysis confirms the impression from Figure 7 that the impact of the day-night temperature offset is to overestimate the tidal amplitude at 97 km and to underestimate it at 104 km. In other words, diurnal tide amplitudes in the upper mesosphere are overestimated at pressure levels where the hour of maximum temperature is during daytime and are underestimated at pressure levels where the temperature maximum is at night. There is no strong impact on the mean amplitude of the semidiurnal tide which, as seen in Figure 18, dominates the temperature variations at 104 km. Comparisons over individual SABER yaw cycles (∼60 days) give similar results because nearly all local times are sampled by then.

[60] Daytime values of [O] are inferred for the T_k algorithm below 90 km based on equilibrium for the partitioning of odd oxygen [O_x], an assumption that is not achieved immediately after sunrise. Nevertheless, the diurnal variations for SABER T_k near 90 km (not shown) indicate continuity after sunrise that is as good as that shown in Figure 18 for higher altitudes. It is also noted that there are likely small offsets in the tidal signatures for the SABER geopotential heights that arise because of an initial tie-in to the heights from the NCEP analyses at 10 hPa, but for a single universal time (UT) time; they have amplitude of up to 30 m at that level. Those offsets occur for both V1.06 and V1.07, but they will have essentially no impact on the much larger amplitude MLT tides. However, they can affect analyses for the tides in the stratosphere and lower mesosphere, if they are conducted on constant altitude rather than pressure surfaces.

5.2. Comparisons With Temperatures From Airglow Measurements

[61] Ground-based mesospheric temperatures have been derived from the nighttime airglow measured in the OH and O_2 rotational bands with the Spectral Airglow Temperature Imager (SATI) instrument at the Sierra Nevada Observatory near Granada (37°N). *Lopez-Gonzalez et al.* [2007] reported on their comparisons with the SABER V1.06 nighttime profiles for the UMLT. They weighted the SABER temper-

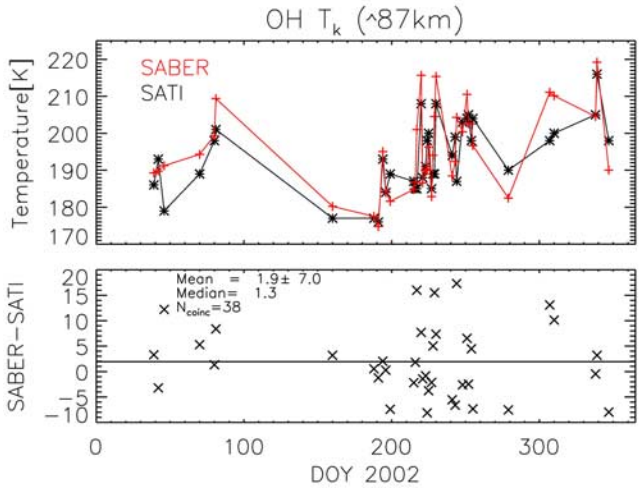

Figure 19. Time series comparison of SABER versus Spectral Airglow Temperature Imager (SATI) temperatures for 2002 for the OH airglow layer centered at 87 km, where the SABER values have been convolved with the vertical weighting function of SATI. The SABER minus SATI values (K) are shown at the bottom, along with their mean and standard deviation.

atures at 87 and 95 km by convolving the SABER T_k profiles with typical airglow emission layers, having a 10 km width at half the emission maximum. For their set of 69 comparison opportunities obtained over 4 years they found SABER minus SATI values of −5.7 ± 7 K at 87 km and 2.5 ± 7 K at 95 km.

[62] Comparisons with the SATI measurements are repeated here, but for the SABER V1.07 temperature profiles of 2002. The SABER/SATI coincidence criteria are ±3 degrees of latitude, ±5 degrees of longitude, and within 1.5 hours in time. The SABER volume emission rate (ver) profiles deduced from its channels 8 and 9 (i.e., 2.0 and 1.6 μm) simultaneous measurements were used to vertically convolve the SABER T_k. Since SABER Ch 8 ver is sensitive to the v = 7–9 OH vibration levels and Ch 9 to v = 3–5 whereas SATI is sensitive to v = 6, we have used an average of the ver from Chs 8 and 9 as convolution functions. The function used for each scan expands 10 km up and down from the OH peak. The convolved SABER T_k was then compared with the SATI OH T_k. The results are very good, as shown in Figure 19. The time series of both data sets indicate good precision; they show similar variations through the nighttime hours and from night-to-night, as well as seasonally. The altitude of the OH peak ranges from 80 to 90 km with an average value of 87.7 ± 2.1 km. The average SABER minus SATI value of T_k is 1.9 K ± 7.0 K, which compares well with the RSS estimates of just the SABER systematic errors of ±1.4 K at 80 km to ±4.0 K at 90 km obtained from Table 2 (without the effects of possible biases for the SABER radiances or for their registration with pressure). The systematic errors in SATI T_k, associated with uncertainties in the modeled OH spectra, are less than ±3 K with a random error of less than 1 K.

[63] For the O_2 airglow emissions of SATI the SABER T_k was convolved with ssian of HWHM of 10 km centered at 95 km. That comparison is shown in Figure 20. The average SABER minus SATI value is 4.9 K ± 10.6 K, which is of the order of the RSS systematic uncertainty of ±3.7 K from Table 2. The systematic errors for SATI T_k from its O_2 spectra are less than ±3 K with a random error of less than 2 K. Thus, the agreement at 95 km is within the combined RSS errors from SABER and SATI.

[64] The Utah State University Mesospheric Temperature Mapper (MTM) is a high-performance, solid state imaging system capable of determining variations in the intensity and rotational temperatures of the two upper mesospheric, near infrared nightglow emissions: the OH (6, 2) Meinel band (peak altitude ~87 km), and the O_2 (0, 1) Atmospheric band emission (peak altitude ~94 km), both of which exhibit well-defined half widths of ~8–10 km [e.g., *Donahue et al.*, 1973; *Baker and Stair*, 1988]. A high quantum efficiency CCD array coupled to a wide-angle telecentric lens system (90° field of view) is used to make sequential narrow band ($\Delta\lambda$ ~1.2 nm) emission measurements using a set of interference filters centered on the OH $P_1(2)$ and $P_1(4)$ lines (at 840 and 846.5 nm) and two well-defined regions of the O_2 (0,1) atmospheric band (at 866 and 868 nm). Each emission is observed for 60 s followed by a background sky measurement at 857 nm, resulting in a ~5.5 min cadence and a pixel footprint at zenith of ~0.9 × 0.9 km at 90 km altitude.

[65] Rotational temperatures are then computed separately using the ratio method as described by *Meriwether* [1984]. The precision of the emission intensity measurements is better than 0.5% (for an individual image) and of the derived rotational temperatures is better than 1–2 K (in 3 min) [*Pendleton et al.*, 2000]. Further details of the MTM data reduction and analysis method are given by *Taylor et al.* [1999, 2001a, 2001b]. Several comparison studies of the MTM temperature data with coincident Na lidar and satellite-borne temperature measurements indicate that the MTM results are accurate to about ±5 K for both the OH and the O_2 data with reference to their nominal emission altitudes of 87 and 94 km, respectively [e.g., *Pendleton et al.*, 2000; *von Savigny et al.*, 2004; *Zhao et al.*, 2005]. Of primary importance to this investigation are the high linearity and stability

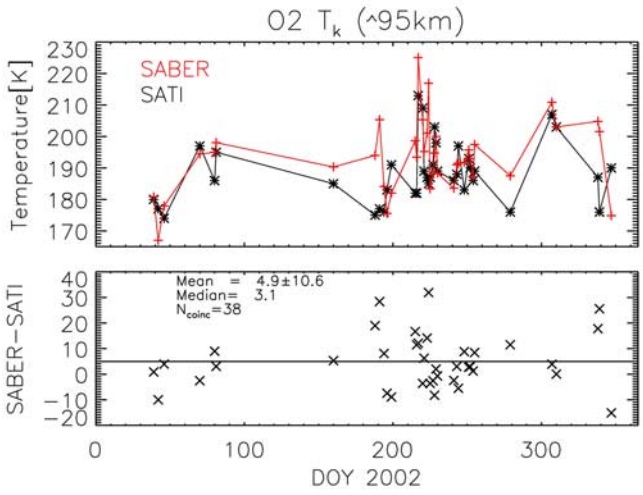

Figure 20. As in Figure 19 but for the O_2 airglow layer centered at 95 km.

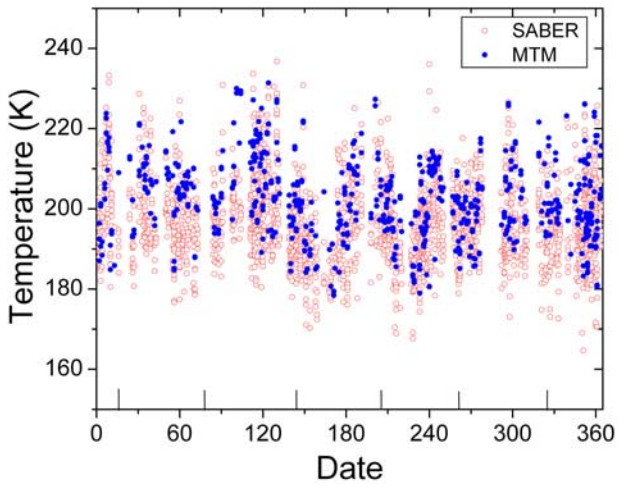

Figure 21. Time series of the SABER T_k (red open circles) and the Mesospheric Temperature Mapper (MTM) OH temperatures (blue solid circles) for 2003 at Maui.

of the MTM, which provide an additional capability for seasonal and long-term investigations of the mesospheric temperature variability [*Taylor et al.*, 2001a, 2001b, 2005].

[66] For the past 5 years (November 2001 to December 2006), the MTM has operated near continuously from the Air Force AMOS facility, located near the summit of Haleakala Crater, Maui, HI (20.8°N, 203.8°E, altitude 2970 m). Autonomous observations were made from dusk to dawn (for solar depression angles >12°) centered on the new moon period resulting in ~22 nights of observations per month. Over 1000 nights of high-quality data have been obtained, providing novel information on the nocturnal and seasonal behavior of mesospheric temperature and its variability.

[67] Figure 21 shows comparison between SABER V1.07 and MTM OH data for 2300 coincidences within 10° latitude and 20° longitude box centered on Maui during 2003. Nocturnal coincidences were obtained over a broad local-time range from 4 to 16 UT throughout the year. The blue solid circles (Figure 21) show the MTM OH temperature averaged over ±12 min centered on the SABER overpass. The red open circles (Figure 21) show the SABER temperatures based on its OH volume emission rate profiles (within ±7.5 km of the peak). For each night, there may be as many as 20 SABER measurements within the selected sample volume. Both data sets show a range of temperatures from 180 to 230 K over the year with a mean of 197.0 K for SABER and 202.2 K for the MTM data. These values are within the expected range of uncertainties for the SABER and the MTM temperatures. More important, the variability of SABER and MTM during the year is tracking well, adding high confidence to the compatibility of the two data sets. Nevertheless, there seems to be a ~5 K systematic offset between these data with the SABER temperatures lower. This difference is investigated further in Figure 22, which shows a histogram of the temperature differences, SABER minus MTM, as determined from Figure 21. The solid curve in Figure 22 shows the Gaussian fit to the data, establishing an offset of 5.8 ± 0.2 K (SABER lower) but with a standard deviation of ±8.9 K.

[68] At this point it is noted that *Oberheide et al.* [2006] found an offset of 7.5 K for their comparisons with OH*(3,1) rotational temperatures at these altitudes at Wuppertal, Germany (51°N, 7°E): SABER temperatures being lower. However, their results were for SABER V1.06. Figures 2b and 12 indicate that the SABER V1.07 temperatures are about 1 to 4 K higher than V1.06 values in that region and ought to provide for better agreement. It is concluded that the SABER V1.07 NLTE algorithm is giving accurate, column-averaged values of T_k for both airglow altitude regions at nighttime.

5.3. Comparisons With Na Lidar Measurements

[69] Ground-based measurements at Fort Collins of laser-induced fluorescence from sodium (Na) atoms provide useful temperature profiles from at least 85 to 100 km geometric altitudes during nighttime and with a vertical resolution of about 2 km [*She et al.*, 2004]. A total of 38 profile comparisons were obtained between SABER V1.07 and the lidar data sets during periods in April, August, and December 2002. Co-location criteria were within 5 degrees latitude, 10 degrees longitude, and 0.5 hours of the lidar hourly means centered on the half hour. Even so, one should realize that the small to medium-scale temperature structure in this region of the atmosphere can change significantly within these space and time windows. Also, it is hard to achieve an actual overlap or a common volume for the limb-viewing SABER versus the more zenith-viewing lidar measurements.

[70] With that in mind, two examples are shown in Figures 23a and 23b, where the numbers of coincidences are 4 and 6, respectively. Figure 23a shows results for day 102 (12 April), while Figure 23b is for day 114 (24 April). Note that both the average lidar (blue diamond) and average SABER (red cross) profiles show vertical structure with larger amplitude on day 114. Horizontal error bars for the lidar data are based on its photon noise, while the SABER bars are its ±1σ standard deviation (SD) values based on the scans that met the co-location criteria. The biggest differ-

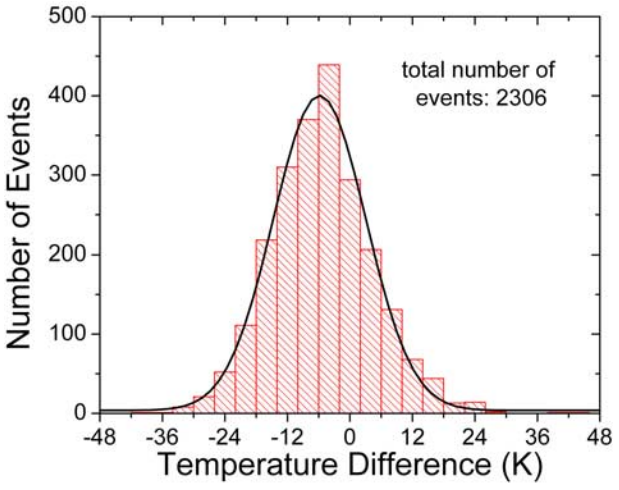

Figure 22. Histogram of the SABER minus MTM temperatures from Figure 21 and a Gaussian fit to them.

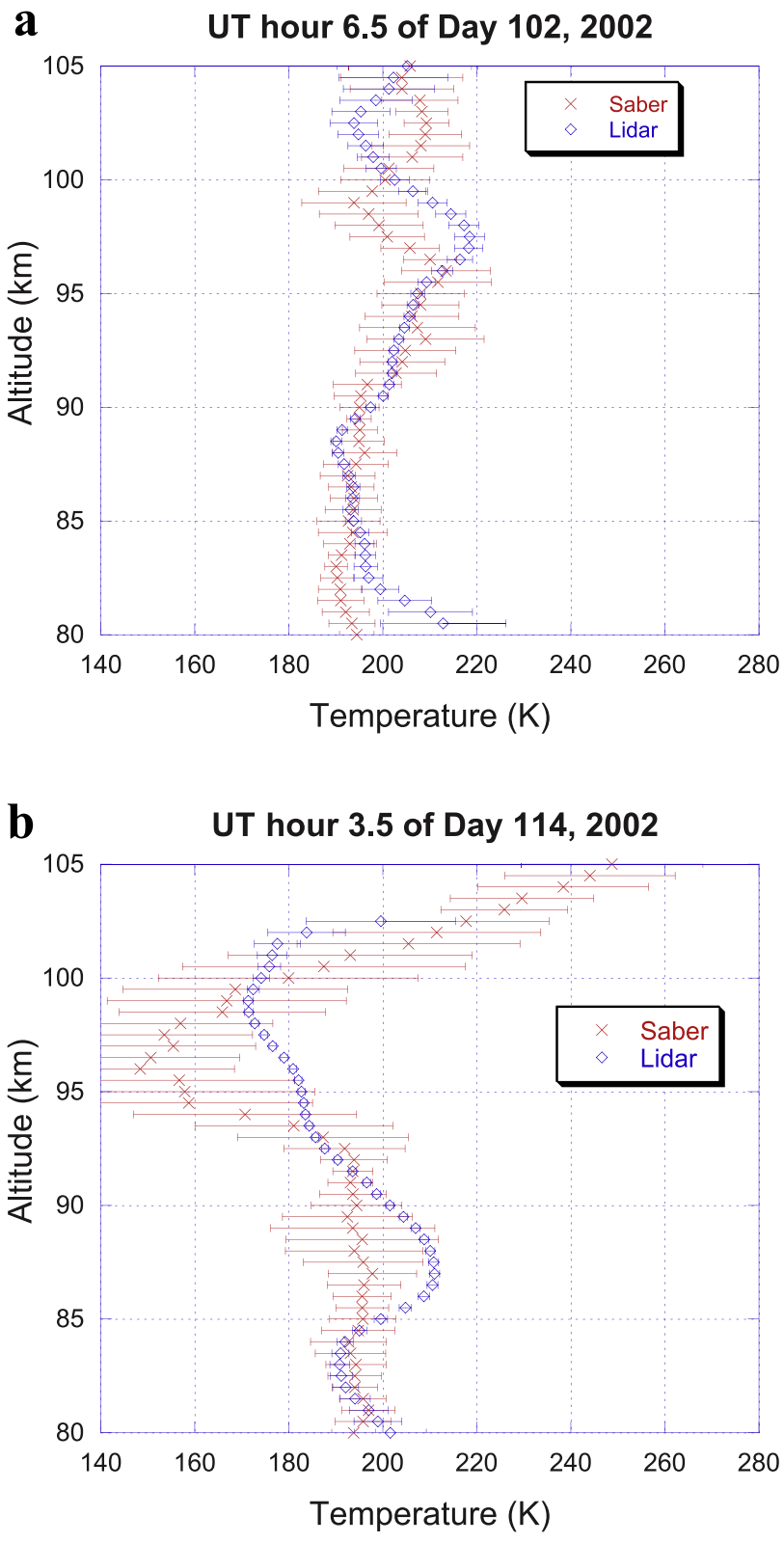

Figure 23. (a) Comparison of the SABER V1.07 versus the Na lidar temperature profiles for day 102 (12 April) of 2002. The lidar profiles are blue (diamonds), and the SABER values are red (crosses). Horizontal bars are the estimates of photon noise error (lidar) and the one standard deviation (SD) variability from the coincident SABER profiles. (b) As in Figure 23a but for day 114 (24 April) of 2002.

Table 3. Mean and SD Differences for T_k From SABER Minus Na Lidar Results[a]

Altitude (km)	April	August	December	Lidar Uncertainty
100	−8.2 (18.1)	4.2 (22.0)	−7.9 (11.7)	3.2
95	−5.1 (8.9)	−1.8 (7.8)	−22.2 (21.3)	1.5
90	−3.6 (7.7)	11.4 (9.6)	−7.6 (9.3)	1.2
85	−2.9 (9.1)	4.8 (7.5)	−6.6 (8.6)	2.2

[a]Units are kelvins.

ences between the SABER and lidar temperatures on day 102 occur between 95 and 105 km. The four coincident SABER profiles are very similar and not exceptional, but with phase variations that are partially responsible for the average difference. It is also important to note that the SD values for the average SABER scan are increasing with altitude, part of which can be explained by the increasing effects of noise for a single SABER profile (see Table 2).

[71] The large-amplitude structure at 95 to 100 km on day 114 in Figure 23b shows up in each of the six separate "coincident" profiles (not shown) that comprise this average SABER profile, although their phases vary somewhat. Each of those profiles has a negative temperature gradient of up to −14 K/km from 93 to 95 km with minimum temperatures in the 120 to 150 K range. The individual profiles, covering a track of about 40 km in longitude and 25 km in latitude, show variations that have vertical wavelengths of roughly 10 km, amplitudes up to 40 K, and periods on the order of an hour. Such large wave amplitudes may be associated with the localized breaking of gravity waves or due to interactions between the migrating tides and stationary planetary waves [*Forbes et al.*, 2006]. Their amplitudes would be reduced somewhat over the averaging time for the lidar measurement.

[72] An investigation of the results for all the days when there were co-located SABER and lidar measurements in April (22 pairings), in August (11 pairings), and in December (5 pairings) shows that the biases for April and August are fairly small, with the possible exception of the results for August at 90 km. The results for December are fewer and more scattered. Table 3 contains the average SABER minus lidar differences for each month and at each altitude. The standard deviations (SD) of the differences are given in parentheses for each case, and the average uncertainties for the lidar measurements due to photon noise are in the last column. By comparing the signed differences (and their SD values) for a given altitude in Table 3 with the RSS of the SABER systematic errors in Table 2, one finds that they agree in some instances but not in others. The SD values are much larger than the random uncertainties for the lidar soundings, and at least part of that difference can be explained by issues of noncoincidence coupled with the significant variability of the atmosphere at these altitudes. In the average the SABER temperatures are lower than those from the lidar at all four altitudes for April and December.

[73] It is concluded then that the findings from the Na lidar comparisons also represent a reasonable validation of the SABER T_k, given that the comparisons in Table 3 are for selected altitudes, as opposed to the column-averaged results of the SATI comparisons of Figures 19 and 20 or the MTM comparisons of Fi ure 22. Furthermore, the good continuity in Figure 18 for the variation of the diurnal tide indicates that the quality of the daytime T_k from SABER is just as good as its nighttime values.

5.4. Comparisons With the Temperature Climatology From Falling Spheres

[74] Retrievals of T_k for the polar summer mesopause region are subject to much larger uncertainties, as reported by Garcia-Comas et al. (submitted manuscript, 2008) and indicated in Table 2. The combined RSS errors for a single profile are of the order of ±9 K between 85 and 90 km and even larger at the higher altitudes. Also, the atmosphere is highly variable in this region during the summer. Therefore it is unreasonable to expect excellent agreement between individual SABER profiles and correlative lidar and/or falling sphere measurements. Instead, we have elected to consider comparisons of July averages of the SABER V1.07 profiles for each year, 2002–2007, versus a 15 July falling sphere climatology based on measurements taken about 10 years earlier [*Lübken*, 1999]. Uncertainties for sphere profiles are about 7 K, 3 K, and 1.5 K at 90, 80, and 70 km, respectively: a small fraction of which is quasi-random for their climatological average. Specifically, Figure 24 shows the average SABER profile from those July means, as obtained from just its profiles at 69 ± 5°N and at 16 ± 20°E; comparisons with SABER zonal average profiles for 65 to 75°N give nearly identical results (not shown). The horizontal bars show the range of the means of the individual years about the average, not the SD of the individual profiles (which is larger). The SABER average agrees with the climatology from about 68 to 86 km, taking into account their combined biases. The mesopause altitude from SABER is lower by 1.5 km and its temperatures are higher than the falling sphere climatology from 86 to 93 km. In addition, the SABER temperatures are lower at 65 km, which

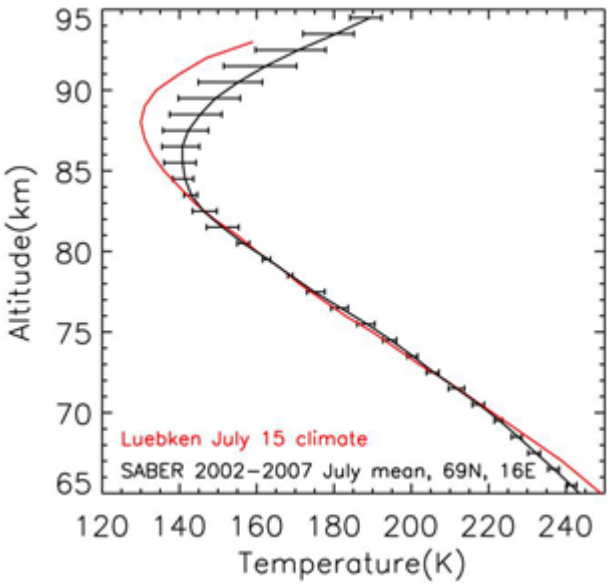

Figure 24. Comparison of SABER temperature profile for July with the falling sphere climatology for 15 July. The SABER profile is its 6-year average, centered at 69°N, 16°E; horizontal bars are the annual differences about the 6-year average.

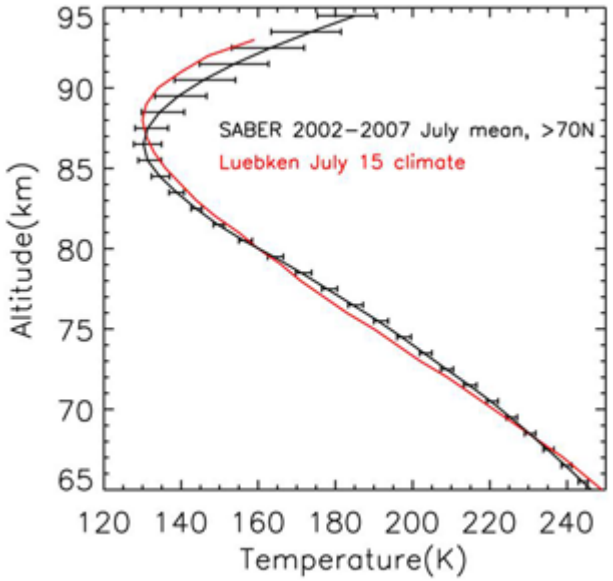

Figure 25. As in Figure 24, but the SABER profile is its 6-year, zonal-mean average, poleward of 70°N for July.

generally agrees with the findings of its comparisons with other correlative measurements for the middle mesosphere.

[75] The SABER measurements in the UMLT region for July at 65 to 70°N are for twilight conditions, and the SABER forward model is based on its assumed nighttime conditions for SZA > 85 degrees. However, it is noted that the meridional temperature gradient is essentially zero poleward of 69°N in the region of the polar mesopause in July [*Lübken et al.*, 2008, and references therein]. Furthermore, nearly every SABER profile for July has SZA < 85 degrees poleward of 70°N. In other words, a comparison of those higher-latitude profiles should provide a useful validation of the SABER daytime algorithm, which makes use of retrieved profiles of [O] at 90 km and below. Figure 25 shows this result; the agreement is improved considerably in the UMLT region, although the altitude of the mesopause from SABER remains 1.5 km lower than that of the climatology.

6. Summary Findings

[76] The approach and findings for the LTE retrievals of SABER $T(p)$ and geopotential height are essentially the same for both the V1.07 and V1.06 data sets, or below about 70 km. The primary sources of systematic error for the SABER LTE $T(p)$ are (1) errors for the measured radiances, (2) biases in the forward model, (3) uncertainties in the corrections for ozone and in the determination of the reference pressure for the retrieved profiles, and (4) not accounting for horizontal gradients in $T(p)$, mainly for the high latitudes during both summer and winter. The simulated effects of the combined random and systematic errors are of order ±1.4 K in the lower stratosphere, ±1 K in the middle stratosphere, and ±2 K in the upper stratosphere and lower mesosphere.

[77] SABER comparisons with the temperature distributions from MIPAS and from the MetO analyses indicate that the SABER temperatur e too high by 2–3 K in the lower stratosphere, but switch to SABER values that are too low by 1 K in the upper stratosphere and by 2–3 K in the midmesosphere. In particular, the excellent quality of the SABER temperatures versus MIPAS is based on a large number of coincident pairings across all latitudes and all seasons. Comparisons with the Rayleigh lidar profiles indicate that SABER is retrieving the vertical structure of the profiles well. The SABER temperatures are higher than the lidar in the lower stratosphere (by 1 to 3 K) but slightly lower from the upper stratosphere to the lower mesosphere (by 1 to 3 K): very similar to its findings versus MIPAS. In the upper mesosphere the SABER temperatures are mostly lower than those from the Rayleigh lidar, but the differences are more variable; however, the average SABER differences versus HALOE are closer to zero at those same altitudes.

[78] The signature of the bias error profiles from the correlative comparisons is similar to the simulated effects of uncertainties for the measured and calculated radiances or their registration with pressure. In effect, the SABER pressures are too large for their corresponding altitudes by 2 to 3 percent. However, no single source of error has been found that accounts for that bias. Some combination of the known errors may be responsible, most likely in the measured radiances and the forward model. Small, negative temperature biases above the region where the pressure registration is performed will lead to slight excesses for the retrieved 9.6-μm ozone and water vapor in the mesosphere and to a lesser extent in the upper stratosphere, as well.

[79] Analyses of T_k in the UMLT region indicate that the retrievals from the SABER NLTE nighttime and daytime algorithms are of good quality. In particular, it was shown that there is continuity within the V1.07 data set for the signature of the diurnal temperature tides at the low latitudes of the UMLT. SABER comparisons with the rotational temperatures derived from the OH and O_2 column airglow emissions with the ground-based SATI instrument near Granada, Spain, and the MTM instrument at Maui, Hawaii, are in agreement with the estimates of bias error for the SABER data set or to within about ±5 K. SABER comparisons with the profiles from the Na lidar at Fort Collins, Colorado, are also in reasonable agreement for specific altitudes within the UMLT, although the SABER values are lower on average. The individual SABER-versus-Na lidar comparisons display more variations than the SABER versus SATI or MTM findings, in part because the lidar comparisons are for specific altitudes and not for an atmospheric column.

[80] Comparisons with the falling sphere climatology for 15 July at 69°N indicate that the SABER temperatures are higher from 86 to 93 km. Similar comparisons, but based on the SABER profiles poleward of 70°N, show better agreement for that same altitude region. Those higher-latitude results indicate that the SABER V1.07 daytime algorithm is providing accurate retrievals of T_k in the UMLT region. It is concluded that the SABER V1.07 temperature distributions can be used to generate the near-global, seasonal and interannual variations of T_k in the UMLT for the period 2002 to the present.

[81] **Acknowledgments.** The authors recognize Chris Mertens, Artem Feofilov, Alexander Kutepov, Richard Picard, Jeremy Winick, and Peter Wintersteiner for their substantial contributions to the development and

testing of the non-LTE temperature algorithms of SABER V1.06 and V1.07. The Rayleigh lidar data used in this publication were obtained as part of the Network for the Detection of Atmospheric Composition Change (NDACC) and are publicly available (see http://www.ndacc.org). The Utah State MTM measurements were made as part of the Maui-MALT program, which is a jointly sponsored initiative between the National Science Foundation (NSF) and the U.S. Air Force Office of Scientific Research (AFOSR) and in coordination with TIMED/SABER measurements. The sodium lidar data used in this publication were obtained with support from the NASA/TIMED project NNX07AB64G and the NSF/CEDAR projects ATM-00-03171 and ATM-0545221. The IAA team was partially supported by the Spanish project ESP2004-01556 and EC FEDER funds. Support for the assessment of the SABER temperature data sets was provided to the SABER project and administered by Charles Holmes (NASA/Headquarters) and Richard Goldberg (NASA/GSFC). The National Center for Atmospheric Research is operated by the University Corporation for Atmospheric Research under sponsorship of the National Science Foundation, and it supports the work of A.K.S.

References

Andrews, D. G., J. R. Holton, and C. B. Leovy (1987), *Middle Atmospheric Dynamics*, 489 pp., Academic, New York.

Baker, D. J., and J. A. T. Stair (1988), Rocket measurements of the altitude distributions of the hydroxyl airglow, *Phys. Scr.*, *37*, 611–622, doi:10.1088/0031-8949/37/4/021.

Donahue, T. M., B. Guenther, and R. J. Thomas (1973), Distribution of atomic oxygen in the upper atmosphere deduced from Ogo 6 airglow observations, *J. Geophys. Res.*, *78*, 6662–6689.

Forbes, J. M., J. Russell, S. Miyahara, X. Zhang, S. Palo, M. Mlynczak, C. J. Mertens, and M. E. Hagan (2006), Troposphere-thermosphere tidal coupling as measured by the SABER instrument on TIMED during July–September 2002, *J. Geophys. Res.*, *111*, A10S06, doi:10.1029/2005JA011492.

Garcia, R. R., and S. Solomon (1994), A new numerical model of the middle atmosphere: 2. Ozone and related species, *J. Geophys. Res.*, *99*, 12,937–12,951.

Garcia, R. R., D. R. Marsh, D. E. Kinnison, B. A. Boville, and F. Sassi (2007), Simulations of secular trends in the middle atmosphere, 1950–2003, *J. Geophys. Res.*, *112*, D09301, doi:10.1029/2006JD007485.

Gille, J. C., and F. B. House (1971), On the inversion of limb radiance measurements, I, Temperature and thickness, *J. Atmos. Sci.*, *28*, 1427–1442, doi:10.1175/1520-0469(1971)028<1427:OTIOLR>2.0.CO;2.

Gille, J. C., and J. M. Russell III (1984), The limb infrared monitor of the stratosphere: Experiment description, performance, and results, *J. Geophys. Res.*, *89*, 5125–5140.

Gille, J. C., et al. (1984), Validation of temperature retrievals obtained by the limb infrared monitor of the stratosphere (LIMS) experiment on NIMBUS 7, *J. Geophys. Res.*, *89*, 5147–5160.

Goldberg, R. A., et al. (2004), The MaCWAVE/MIDAS rocket and ground-based measurements of polar summer dynamics: Overview and mean state structure, *Geophys. Res. Lett.*, *31*, L24S02, doi:10.1029/2004GL019411.

Gordley, L. L., B. T. Marshall, and D. A. Chu (1994), LINEPAK: Algorithms for modeling spectral transmittance and radiance, *J. Quant. Spectrosc. Radiat. Transfer*, *52*, 563–580, doi:10.1016/0022-4073(94)90025-6.

Gusev, O., M. Kaufmann, U.-K. Grossmann, F. J. Schmidlin, and M. G. Shepherd (2006), Atmospheric neutral temperature distribution at the mesopause altitude, *J. Atmos. Sol. Terr. Phys.*, *68*, 1684–1697, doi:10.1016/j.jastp.2005.12.010.

Hedin, A. E. (1991), Extension of the MSIS thermosphere model into the middle and lower atmosphere, *J. Geophys. Res.*, *96*, 1159–1172.

Hervig, M. E., et al. (1996), Validation of temperature measurements from the Halogen Occultation Experiment, *J. Geophys. Res.*, *101*, 10,277–10,285.

Kaufmann, M., O. A. Gusev, K. U. Grossmann, R. G. Roble, M. E. Hagan, C. Hartsough, and A. A. Kutepov (2002), The vertical and horizontal distribution of CO_2 densities in the upper mesosphere and lower thermosphere as measured by CRISTA, *J. Geophys. Res.*, *107*(D23), 8182, doi:10.1029/2001JD000704.

Kutepov, A. A., A. G. Feofilov, B. T. Marshall, L. L. Gordley, W. D. Pesnell, and R. A. Goldberg (2006), SABER temperature observations in the summer polar mesosphere and lower thermosphere: Importance of accounting for the CO_2 ν_2 quanta V-V exchange, *Geophys. Res. Lett.*, *33*, L21809, doi:10.1029/2006GL026591.

LeBlanc, T., I. S. McDermid, P. Keckhut, A. Hauchecorne, C. Y. She, and D. A. Kreuger (1998), Temperature climatology of the middle atmosphere from long-term lidar measurements at middle and low latitudes, *J. Geophys. Res.*, *103*, 17,191–17,204.

Lopez-Gonzalez, M. J., et al. (2007), Ground-based mesospheric temperatures at mid-latitude derive O_2 and OH airglow SATI data: Comparison with SABER measurements, *J. Atmos. Sol. Terr. Phys.*, *69*, 2379–2390, doi:10.1016/j.jastp.2007.07.004.

Lopez-Puertas, M., M. A. Lopez-Valverde, R. R. Garcia, and R. G. Roble (2000), A review of CO_2 and CO abundances in the middle atmosphere, in *Atmospheric Science Across the Stratopause*, *Geophys. Monogr. Ser.*, vol. 123, edited by D. E. Siskind et al., pp. 83–100, AGU, Washington, D. C.

Lopez-Puertas, M., et al. (2004), Evidence for an OH (v) excitation mechanism of CO_2 4.3 μm nighttime emission from SABER/TIMED measurements, *J. Geophys. Res.*, *109*, D09307, doi:10.1029/2003JD004383.

Lübken, F.-J. (1999), Thermal structure of the Arctic summer mesosphere, *J. Geophys. Res.*, *104*, 9135–9149.

Lübken, F.-J., G. Baumgarten, J. Fiedler, M. Gerding, J. Hoeffner, and U. Berger (2008), Seasonal and latitudinal variation of noctilucent cloud altitudes, *Geophys. Res. Lett.*, *35*, L06801, doi:10.1029/2007GL032281.

Manney, G. L., et al. (2005), Diagnostic comparison of meteorological analyses during the 2002 Antarctic winter, *Mon. Weather Rev.*, *133*, 1261–1278, doi:10.1175/MWR2926.1.

Manney, G. L., et al. (2008a), The high Arctic in extreme winters: Vortex, temperature, and MLS and ACE-FTS trace gas evolution, *Atmos. Chem. Phys.*, *8*, 505–522.

Manney, G. L., et al. (2008b), The evolution of the stratopause during the 2006 major warming: Satellite data and assimilated meteorological analyses, *J. Geophys. Res.*, *113*, D11115, doi:10.1029/2007JD009097.

Marshall, B. T., L. L. Gordley, and D. A. Chu (1994), Bandpak: Algorithms for modeling broadband transmission and radiance, *J. Quant. Spectrosc. Radiat. Transfer*, *52*, 581–599, doi:10.1016/0022-4073(94)90026-4.

Meriwether, J. W., Jr. (1984), Ground based measurements of mesospheric temperatures by optical means, in *Map Handbook*, vol. 13, pp. 1–18, Univ. of Ill. at Urbana-Champaign.

Mertens, C. J. (2008), Kinetic temperature and carbon dioxide from broadband infrared limb emission measurements taken from the TIMED/SABER instrument, *Adv. Space Res.*, doi:10.1016/j.asr.2008.04.017, in press.

Mertens, C. J., M. G. Mlynczak, M. Lopez-Puertas, P. P. Wintersteiner, R. H. Picard, J. R. Winick, and L. L. Gordley (2001), Retrieval of mesospheric and lower thermospheric kinetic temperature from measurements of CO_2 15 μm Earth limb emission under non-LTE conditions, *Geophys. Res. Lett.*, *28*(7), 1391–1394.

Mertens, C. J., M. G. Mlynczak, M. Lopez-Puertas, P. P. Wintersteiner, R. H. Picard, J. R. Winick, and L. L. Gordley (2002), Retrieval of the kinetic temperature and carbon dioxide abundance from non-local thermodynamic equilibrium limb emission measurements made by the SABER experiment on the TIMED satellite, in Remote Sensing of Clouds and the Atmosphere VII, *Proc. SPIE Int. Soc. Opt. Eng.*, *48882*, 162–171.

Mertens, C. J., et al. (2004), SABER observations of mesospheric temperatures and comparisons with falling sphere measurements taken during the 2002 summer MaCWAVE campaign, *Geophys. Res. Lett.*, *31*, L03105, doi:10.1029/2003GL018605.

Niro, F., T. von Clarmann, K. Jucks, and M. J.-Hartmann (2005), Spectra calculations in central and wing regions of CO_2 IR bands between 10 and 20 μm: III. Atmospheric emission spectra, *J. Quant. Spectrosc. Radiat. Transfer*, *90*, 61–76, doi:10.1016/j.jqsrt.2004.04.005.

Oberheide, J., D. Offermann, and M. G. Mlynczak (2006), Intercomparison of kinetic temperature from 15 μm CO_2 limb emissions and OH* (3,1) rotational temperature in nearly coincident air masses: SABER, GRIPS, *Geophys. Res. Lett.*, *33*, L14811, doi:10.1029/2006GL026439.

Pendleton, W. R., Jr., M. J. Taylor, and L. C. Gardner (2000), Terdiurnal oscillations in OH Meinel rotational temperatures for fall conditions at northern midlatitude sites, *Geophys. Res. Lett.*, *27*, 1799–1802.

Picone, J. M., A. E. Hedin, D. P. Drob, and A. C. Aikin (2002), NRLMSISE-00 empirical model of the atmosphere: Statistical comparisons and scientific issues, *J. Geophys. Res.*, *107*(A12), 1468, doi:10.1029/2002JA009430.

Preusse, P., et al. (2006), Tropopause to mesopause gravity waves in August: Measurement and modeling, *J. Atmos. Sol. Terr. Phys.*, *68*, 1730–1751, doi:10.1016/j.jastp.2005.10.019.

Randel, W., et al. (2004), The SPARC intercomparison of middle-atmosphere climatologies, *J. Clim.*, *17*, 986–1003, doi:10.1175/1520-0442(2004)017<0986:TSIOMC>2.0.CO;2.

Remsberg, E., et al. (2002), An assessment of the quality of Halogen Occultation Experiment temperature profiles in the mesosphere based on comparisons with Rayleigh backscatter lidar and inflatable falling sphere measurements, *J. Geophys. Res.*, *107*(D20), 4447, doi:10.1029/2001JD001521.

Remsberg, E., G. Lingenfelser, V. L. Harvey, W. Grose, J. Russell III, M. Mlynczak, L. Gordley, and B. T. Marshall (2003), On the verification of the quality of SABER temperature, geopotential height, and wind

fields by comparison with Met Office assimilated analyses, *J. Geophys. Res.*, *108*(D20), 4628, doi:10.1029/2003JD003720.

Remsberg, E. E., L. L. Gordley, B. T. Marshall, R. E. Thompson, J. Burton, P. Bhatt, V. L. Harvey, G. Lingenfelser, and M. Natarajan (2004), The Nimbus 7 LIMS version 6 radiance conditioning and temperature retrieval methods and results, *J. Quant. Spectrosc. Radiat. Transfer*, *86*, 395–424, doi:10.1016/j.jqsrt.2003.12.007.

Remsberg, E., G. Lingenfelser, M. Natarajan, L. Gordley, B. T. Marshall, and E. Thompson (2007), On the quality of the Nimbus 7 LIMS version 6 ozone for studies of the middle atmosphere, *J. Quant. Spectrosc. Radiat. Transfer*, *105*, 492–518, doi:10.1016/j.jqsrt.2006.12.005.

Ridolfi, M., et al. (2007), Geophysical validation of temperature retrieved by the ESA processor from MIPAS/ENVISAT atmospheric limb-emission measurements, *Atmos. Chem. Phys.*, *7*, 4459–4487.

Roble, R. G., and E. C. Ridley (1994), A thermosphere-ionosphere-mesosphere-electrodynamics general circulation model (time-GCM): Equinox solar cycle minimum simulations (30–500 km), *Geophys. Res. Lett.*, *21*, 417–420.

Rothman, L. S., et al. (2003), The HITRAN molecular spectroscopic database: Edition of 2000 including updates through 2001, *J. Quant. Spectrosc. Radiat. Transfer*, *82*, 5–44, doi:10.1016/S0022-4073(03)00146-8.

Rothman, L. S., et al. (2005), The HITRAN 2004 molecular spectroscopic database, *J. Quant. Spectrosc. Radiat. Transfer*, *96*, 139–204, doi:10.1016/j.jqsrt.2004.10.008.

Russell, J. M., III, et al. (1993), The Halogen Occultation Experiment, *J. Geophys. Res.*, *98*, 10,777–10,797.

Russell, J. M., III, M. G. Mlynczak, L. L. Gordley, J. Tansock, and R. Esplin (1999), An overview of the SABER experiment and preliminary calibration results, *Proc. SPIE Int. Soc. Opt. Eng.*, *3756*, 277–288.

Schwartz, M. J., et al. (2008), Validation of the AURA microwave limb sounder temperature and geopotential height measurements, *J. Geophys. Res.*, *113*, D15S11, doi:10.1029/2007JD008783.

Sharma, R. D., and P. P. Wintersteiner (1990), Role of carbon dioxide in cooling planetary atmospheres, *Geophys. Res. Lett.*, *17*, 2201–2204.

She, C. Y., et al. (2004), Tidal perturbations and variability in the mesopause region over Fort Collins, Colorado (41°N, 105°W): Continuous multiday temperature and wind lidar observations, *Geophys. Res. Lett.*, *31*, L24111, doi:10.1029/2004GL021165.

Shine, K. P., J. J. Barnett, and W. J. Randel (2008), Temperature trends derived from Stratospheric Sounding Unit radiances: The effect of increasing CO_2 on the weighting function, *Geophys. Res. Lett.*, *35*, L02710, doi:10.1029/2007GL032218.

Sica, R. J., et al. (2008), Validation of the Atmospheric Chemistry Experiment (ACE) version 2.2 temperature using ground-based and space-borne measurements, *Atmos. Chem. Phys.*, *8*, 35–62.

Taylor, M. J., W. R. Pendleton Jr., C. S. Gardner, and R. J. States (1999), Comparison of terdiurnal tidal oscillations in mesospheric OH rotational temperature and Na lidar temperature measurements at mid-latitudes for fall/spring conditions, *Earth Planets Space*, *51*, 877–885.

Taylor, M. J., L. C. Gardner, and W. R. Pendleton Jr. (2001a), Long period wave signatures in mesospheric OH Meinel (6, 2) band intensity and rotational temperature at mid latitudes, *Adv. Space Res.*, *27*, 1171–1179, doi:10.1016/S0273-1177(01)00153-3.

Taylor, M. J., W. R. Pendleton Jr., H. L. Liu, C. Y. She, L. C. Gardner, R. G. Roble, and V. Vasoli (2001b), Large amplitude perturbations in mesospheric OH Meinel and 87-km Na lidar temperatures around the autumnal equinox, *Geophys. Res. Lett.*, *28*, 1899–1902.

Taylor, M. J., A. Taori, D. R. Hatch, H. L. Liu, and R. G. Roble (2005), Characterization of the semi-annual-oscillation in mesospheric temperatures at low-latitudes, *Adv. Space Res.*, *35*, 2037–2043, doi:10.1016/j.asr.2005.05.111.

von Savigny, C., et al. (2004), First near-global retrievals of OH rotational temperatures from satellite-based Meinel band emission measurements, *Geophys. Res. Lett.*, *31*, L15111, doi:10.1029/2004GL020410.

Zhao, Y., M. J. Taylor, and X. Chu (2005), Comparison of simultaneous Na lidar and Mesospheric Temperature Mapper measurements and the effects of tides on the emission layer heights, *J. Geophys. Res.*, *110*, D09S07, doi:10.1029/2004JD005115.

C. Brown, L. L. Gordley, B. T. Marshall, and R. E. Thompson, G & A Technical Software, Inc., Newport News, VA 23606, USA.

M. Garcia-Comas, M. J. Lopez-Gonzalez, and M. Lopez-Puertas, Instituto de Astrofisica de Andalucia, CSIC, Granada E-18008, Spain.

D. Krueger and C.-Y. She, Department of Physics, Colorado State University, Fort Collins, CO 80523, USA.

G. S. Lingenfelser and J. Martin-Torres, Science Systems and Applications, Inc., Hampton, VA 23666, USA.

M. G. Mlynczak and E. E. Remsberg (corresponding author), Science Directorate, NASA Langley Research Center, 21 Langley Boulevard, Mail Stop 401B, Hampton, VA 23681-2199, USA. (ellis.e.remsberg@nasa.gov)

J. M. Russell III, Center for Atmospheric Sciences, Hampton University, Hampton, VA 23668, USA.

A. K. Smith, National Center for Atmospheric Research, Boulder, CO 80307, USA.

M. J. Taylor and Y. Zhao, Center for Atmospheric and Space Sciences, Utah State University, Logan, UT 84322, USA.